Biochemical Pharmacology 247 (2026) 117807

Contents lists available at ScienceDirect

Biochemical Pharmacology

journal homepage: www.elsevier.com/locate/biochempharm

The rare bile acid isoallolithocholic acid (IALCA) is an EphA2 antagonist sparing FXR and TGR5 receptors

Andrea Blesio [a], Carmine Giorgio [a], Francesca Romana Ferrari [a], Stefano Sala [a], Lisa Flammini [a], Ilaria Zanotti [a], Daniela Passeri [b], Antimo Gioiello [c], Lorenzo Sarcone [a], Riccardo Castelli [a], Kun Karnchanapandh [a], Federica Vacondio [a], Lorenzo Tagliazucchi [a], Laura Scalvini [a], Marco Mor [a], Alessio Lodola [a,*], Massimiliano Tognolini [a,*]

[a] Dipartimento di Scienze degli Alimenti e del Farmaco, Università degli Studi di Parma, Parma, Italy
[b] Tes Pharma S.r.l., 6073 Solomeo Corciano, Italy
[c] Dipartimento di Scienze Farmaceutiche, Università degli Studi di Perugia, Perugia, Italy

ARTICLE INFO

Keywords:
Bile acid
Isoallolithocholic acid
EphA2
Ephrin
Receptor
Drug discovery

ABSTRACT

The role of the Eph/ephrin system is well recognized in various physiological and pathological processes, including acute inflammation and cancer. We previously discovered that the secondary bile acid lithocholic acid (LCA) is a competitive antagonist of Eph receptors. The utility of LCA as a pharmacological tool for investigating Eph/ephrin biology was hampered by its primary activity at the FXR and TGR5 receptors. A recent study of centenarians' gut microbiomes revealed that a rare bile acid closely related to LCA, isoallolithocholic acid (IALCA), exerts marked protective effects on the intestinal epithelium, but its specific molecular target was unidentified. Considering the well-documented involvement of EphA2 in regulating intestinal epithelial/endothelial permeability, we asked whether IALCA could act through this receptor. Molecular docking and dynamics simulations predicted that IALCA binds within the ephrin-A1–binding pocket of EphA2. Our findings were validated through wet experiments, and IALCA emerged as a selective EphA2 inhibitor, blocking ephrin-A1 binding with low-micromolar potency. In functional studies, IALCA inhibited ephrin-A1–induced EphA2 phosphorylation, cell retraction, and rounding, confirming its antagonistic activity. Moreover, IALCA showed no detectable activity at the classical bile-acid receptors FXR, PXR, LXRα, or TGR5, thereby potentially linking its cellular and phenotypic effects to modulation of the Eph–ephrin system. As a final step, we demonstrated that IALCA also provides an attractive template for synthesizing new Eph antagonists. Overall, this work underscores the potential of the human gut microbiome as a reservoir of privileged chemical scaffolds for both fundamental pharmacology and therapeutic drug development.

Abbreviations: 5AR, 5α-reductase; AKT, protein kinase B; ASBT, Apical Sodium-dependent Bile Acid Transporter; BA, Bile Acid; BSA, Bovine Serum Albumin; CBAH, conjugated bile acid hydrolase; CDCA, chenodeoxycholic acid; DCA, deoxycholic acid; DMEM, Dulbecco's Modified Eagle Medium; DMSO, Dimethyl sulfoxide; DPBS, Dulbecco's Phosphate-Buffered Saline; EMEM, Eagle's Minimum Essential Medium; Eph, Erythropoietin-producing hepatocellular receptor; ERK, Extracellular signal Regulated Kinases; FBS, Fetal Bovine Serum; Fc, Fragment crystallizable region; FNIII, Fibronectin type III; FOXP3, Forkhead Box P3; FXR, Farnesoid X receptor; H-H, Head-to-head; HRP, Horseradish Peroxidase; H-T, Head-to-Tail; IALCA, Isoallolithocholic Acid; IC_{50}, Half maximal inhibitory concentration; LBD, Ligand Binding Domain; LCA, Lithocholic Acid; LXRα, Liver X receptor alfa; LDH, Lactate Dehydrogenase; MTT, 3-[4,5-dimethylthiazol-2-yl]-2,5 diphenyl tetrazolium bromide; MD, molecular dynamics; NEAA, Non-essential amino acids; NR4A1, Nuclear Receptor subfamily 4 group A member 1; PBS, Phosphate Buffered Saline; PC3, human prostate adenocarcinoma cells; PDZ, Post-synaptic density 95, Disks-large and Zonula occludens-1; PI3K, Phosphatidylinositol 3-Kinase; PXR, Pregnane X receptor; RAS, Rat Sarcoma Virus; RMSD, root-mean-square deviation; RT, Room temperature; RTK, Receptor Tyrosine Kinase; SAR, Structure-activity relationship; S.D., Standard Deviation; TCA, taurocholic acid; TGR5, G protein-coupled bile acid receptor 1; Tyr, Tyrosine.

* Corresponding authors.
E-mail addresses: alessio.lodola@unipr.it (A. Lodola), massimiliano.tognolini@unipr.it (M. Tognolini).

https://doi.org/10.1016/j.bcp.2026.117807
Received 18 December 2025; Received in revised form 2 February 2026; Accepted 11 February 2026
Available online 13 February 2026
0006-2952/© 2026 The Author(s). Published by Elsevier Inc. This is an open access article under the CC BY license (http://creativecommons.org/licenses/by/4.0/).

1. Introduction

Erythropoietin-producing hepatocellular receptors (Ephs) represent the leading subfamily of receptor tyrosine kinases (RTKs). Based on their sequence homology and ligand specificity, they are categorized in two different subclasses: EphAs and EphBs. Fourteen members are currently known to be present in the human genome, nine EphA receptor subtypes (EphA1-A8 and Eph10) and five EphB receptor subtypes (EphB1-B4 and EphB6) [1,2].

Eph receptors are composed of three main regions: 1) the N-terminal extracellular section, that is in turn composed of a globular ligand-binding domain (LBD), a cysteine-rich region and two fibronectin type III repeats (FNIII) domains; 2) a transmembrane (TM) domain; 3) a cytoplasmic portion, that includes the tyrosine kinase domain, a Sterile Alpha Motif (SAM), and a PDZ-binding motif [3].

Physiological activation of Eph receptors occurs through membrane-associated ephrin ligands, which are classified in ephrin-As and ephrin-Bs, based on their sequence homology and structure. Both classes present an extracellular receptor-binding domain (RBD) which is linked to the membrane through a glycosylphosphatidylinositol (GPI)-anchored moiety in case of ephrin-As, and by a transmembrane domain associated with a PDZ-binding motif in the case of ephrin-Bs [3,4].

EphA receptors typically bind GPI-anchored ephrin-A ligands, whereas EphB receptors preferentially engage transmembrane ephrin-B ligands. However, this class-based specificity is not absolute, with several well-documented exceptions involving cross-class interactions. [5,6].

Unlike most receptor–ligand systems, Eph–ephrin complexes mediate bidirectional signaling that transduces information into both the receptor-expressing and ligand-expressing cells. In the receptor-bearing cell, forward signaling is initiated by ligand-dependent receptor clustering, leading to autophosphorylation of conserved tyrosines in the kinase domain. These phosphotyrosine motifs in turn work as recruitment platforms for downstream effectors, thereby activating typical RTK signaling pathways. [7]. In contrast, ephrin-B ligands-mediated reverse signaling relies on their conserved cytoplasmic tail, which contains a C-terminal PDZ-binding motif and multiple tyrosine residues. The phosphorylation of these domains by Src-family kinases engages PDZ-domain proteins and other adaptors.

While initially recognized for their roles in developmental processes such as axon guidance and tissue patterning, Eph receptors and ephrins have subsequently emerged as critical regulators of adult tissue homeostasis [8], including the maintenance of intestinal tissue integrity through the control of intestinal stem cells and progenitor cells behavior [9]. Eph receptors play a well-established, homeostatic role in epithelial differentiation, proliferation and migration, but their signaling is context-dependent [10]. Indeed, it can be protective under steady-state conditions but could be detrimental during inflammation or injury [11].

The Eph-ephrin system is greatly investigated in oncology [12], where EphA2 emerged as the most promising target being overexpressed in various solid tumors, including colon, breast, prostate, lung, melanoma and glioblastoma [1,13]. Several options for targeting EphA2 are currently under investigation: small molecules based on amino acid conjugates of lithocholic acid, targeted nanoparticles, bicyclic peptides linked to chemotherapeutic agents and monoclonal antibodies, but so far none of these approaches reached the clinical approval [1].

Our research group has been investigating the Eph-ephrin system and its modulators since 2011. The screening of a bile acids (BAs) chemical collection available at the University of Parma led to the identification of **3α-hydroxy-5β-cholan-24-oic acid** (lithocholic acid, LCA, Fig. 1) as a weak binder of the Eph receptors able to inhibit Ephs activation induced by ephrin ligands [14]. LCA is a secondary BA produced by specific 7α-dehydroxylating gut bacteria, acting on the primary BA chenodeoxycholic acid [15].

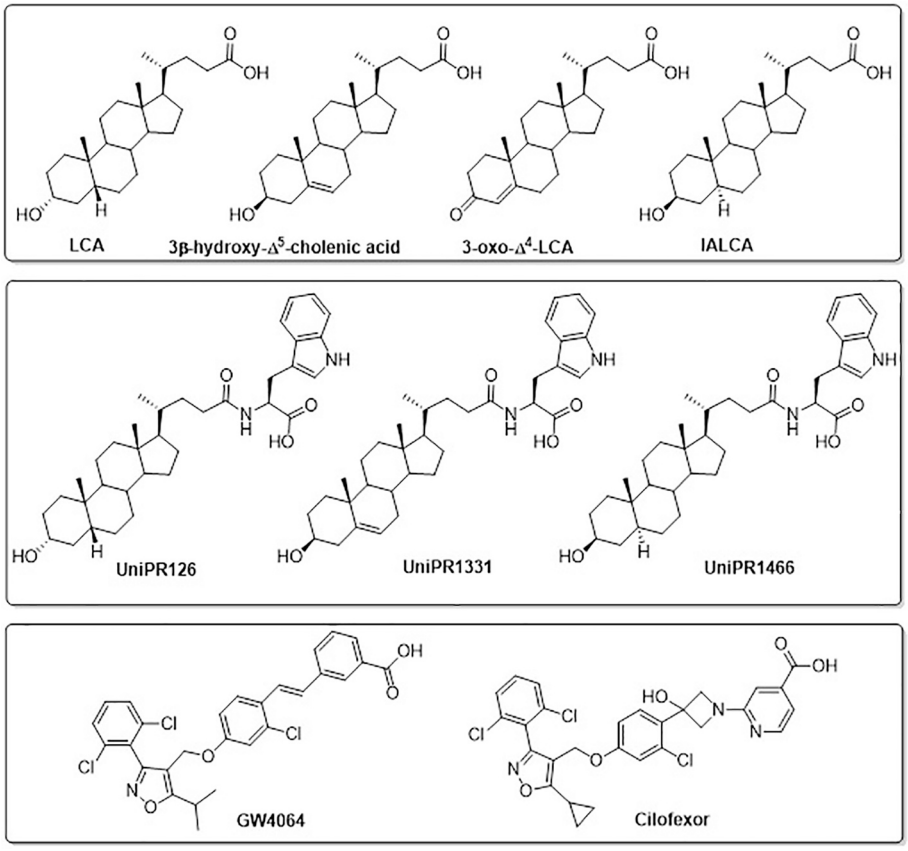


Fig. 1. Chemical structures of selected BAs, BA L-Trp conjugates and reference dual FXR/EphA2 ligands. UniPR1466 structure is described here for the first time.

Given the positive results obtained with LCA, we further investigated and characterized the structure–activity relationship (SAR) of (5β)-cholan-24-oic acid derivatives [16]. During this research, we discovered 3β-hydroxy-Δ^5-cholenic acid, a secondary metabolite generated in the "alternative pathway" connecting cholesterol to primary BAs, as a slightly more potent EphA2 antagonist than LCA [17]. Thus, bile acids emerged as an effective "reservoir" of EphA2 binders, with an intriguing biological activity. What is more, not only bile acids (BA) themselves, but also their synthetic L-Trp conjugates such as UniPR126 and UniPR1331 (Castelli et al, 2015 and Fig. 1) emerged as potent and yet effective EphA2 receptor antagonists. In this context, microbially amidated bile acids (MABAs), which are minor BA amino acid conjugates (mainly involving leucine, phenylalanine, tyrosine and tryptophane) produced by gut microbiota may emerge as physiological or pathological modulators of the Eph-Ephrin system. MABAs have also emerged in patients as key biomarkers in the hepatopancreatobiliary disorders, confirming their relevance as bioactive compounds [18].

The microbiome profile has gained growing interest also as a key player in the health status of individuals. New discoveries highlighted a distinct gut microbiome in centenarians, revealing that their microbiome includes bacteria that generate unique secondary BAs. One of them, **3β-hydroxy-5α-cholan-24-oic acid** (isoalloLCA, IALCA, Fig. 1), generated by the key intermediate 3-oxo-Δ^4-LCA, through the activity of 3-oxo-Δ^4-5α-reductase [19], reaches significant levels in the gut of centenarians, contributing to intestinal homeostasis maintenance [20].

IALCA has gained relevance for its capacity to reduce inflammation by stimulating the immune system, inducing the differentiation of naive T cells into T_{reg} cells by indirectly activating NR4A1, an orphan nuclear receptor involved in inflammatory responses [21]. Moreover, IALCA has been found to alleviate acute intestinal inflammation by metabolically reprogramming macrophages [22]. Despite these robust anti-inflammatory effects in multiple models, the identification of the specific molecular target(s) of IALCA remains elusive.

In light of the pharmacophoric elements possessed by IALCA, i.e. a flat and rigid 5α-androstane structure and a carboxylic acid group at a suitable distance, we hypothesized that this compound could bind and modulate the activity of the Eph-ephrin signaling system, while sparing the physiological receptors of traditional BAs (including LCA), such as nuclear farnesoid X receptors (FXRs), pregnane X receptor (PXR) and membrane TGR5 receptor [25].

In the present work, we report a full chemical and pharmacological characterization of IALCA as a new modulator of the EphA2 receptor in cell-free and cell-based experiments, with remarkably higher potency than that dual FXR/EphA2 ligands (LCA, GW4064 and Cilofexor, Fig. 1) and its use as template structure to generate effective amino-acid conjugates able to interfere with the Eph-ephrin system.

2. Materials and methods

2.1. Reagents

Culture media and supplements were from Euroclone (Milan, Italy). Recombinant proteins and antibodies were supplied by R&D System (Minneapolis, MN, USA). Leupeptin, aprotinin, NP40, Tween20, BSA, and salts for solution were purchased from ITW Reagents (Chicago, IL, USA). EDTA and sodium orthovanadate were provided by Merck (Darmstadt, Germany). IALCA (Cayman Chemical, Ann Arbor, MI, USA #29542) were stocked in dimethyl sulfoxide (DMSO) (Honeywell, Charlotte, NC, USA, #51779) at 10 mM.

2.2. Cell cultures

PC3 human prostate adenocarcinoma cells (ECACC, Salisbury, UK) were cultured in Ham's F12 supplemented with 7% FBS and 1% antibiotic solution and were maintained in humidified atmosphere enriched with 5% CO_2 at 37 °C.

2.3. ELISA binding assays

Displacement assays were carried out to evaluate IALCA's ability to prevent biotinylated ephrin-A1-Fc binding to EphA2-Fc. Ninety-six-wells ELISA Costar® high-binding plate (Corning, NY, USA, #9018) was incubated overnight at 4 °C with 100 μL/well of 1 μg/mL EphA2-Fc (R&D Systems, Minneapolis, MN, USA, #639A2) diluted in sterile PBS (0.2 g/L KCl, 8.0 g/L NaCl, 0.2 g/L KH_2PO_4, 1.15 g/L Na_2HPO_4, pH 7.4). The next day, the plate was washed three times with washing buffer (0.05% Tween20 in PBS, pH 7.4) and incubated with blocking solution (1% BSA in PBS) for 1 h at 37 °C. Following three washes, IALCA was added at proper concentrations in 0.5% DMSO in PBS and incubated for 1 h at 37 °C. Next, biotinylated ephrin-A1-Fc (R&D Systems, Minneapolis, MN, USA, #BT602) was added at the concentration of its calculated K_D value and incubated for 4 h at 37 °C. The plate was washed three times and incubated with Streptavidin-HRP (Merck, Darmstadt, Germany, #S5512) solution for 20 min at room temperature. Then, the plate was washed again for three times and incubated with TMB tetramethylbenzidine (Merck, Darmstadt, Germany, #860336). The reaction was stopped with 100 μL/well of HCl 3 N and the absorbance was measured using Sunrise Tecan plate reader (Tecan, Männedorf, Switzerland). The IC_{50} values were determined using one-site competition non-linear regression analysis with Prism software (GraphPad Software Inc., La Jolla, CA, USA).

To determine the K_i value of IALCA towards biotinylated ephrin-A1-Fc binding to EphA2-Fc, saturation assays were carried out. The protocol is similar to the displacement assay described above, with the only exception that biotinylated ephrin-A1-Fc was added in a range from 1 to 2000 ng/mL. Incubation time was extended to 5 h, at 37 °C. The K_i values were determined using one-site competition non-linear regression analysis with Prism software (GraphPad Software Inc., La Jolla, CA, USA).

In order to evaluate IALCA's preferential binding to Eph receptors family members, selectivity assays were performed. Ninety-six-wells ELISA Costar® high-binding plate (Corning, Corning, NY, USA, #9018) was incubated overnight at 4 °C with 100 μL/well of 1 μg/mL of various EphAs-Fc and EphBs-Fc receptors (R&D Systems, Minneapolis, MN, USA) diluted in sterile PBS. The physiological ligands of each receptor type were used at their K_D value; biotinylated ephrin-A1-Fc (R&D Systems, Minneapolis, MN, USA, #BT602) was added for EphAs, whilst biotinylated ephrin-B1-Fc (R&D Systems, Minneapolis, MN, USA, #BT374) was used for EphB receptors. The assay was performed following displacement assay protocol, as described above.

2.4. Nuclear receptor selectivity

Assays to evaluate compound selectivity against key nuclear receptors (PXR, LXR, FXR) were performed in white, low-volume 384-well ProxiPlates (PerkinElmer Waltham, MA, USA #6008280) using a final volume of 15 μL *per* well. Each well contained the corresponding GST-tagged nuclear receptor ligand binding domain (NR-LBD) protein and its biotinylated coactivator peptide, both used at specific, previously optimized concentrations. GST-NR-LBD protein and biotinylated coactivator peptide were incubated with concentration response of compounds from 0.001 μM to 100 μM for 1 h at rt. Subsequently, a detection mix of acceptor and donor beads was added. After 4 h of incubation at room temperature, luminescence was measured using an EnVision reader.

2.5. TGR5 activity

TGR5 activation was assessed by measuring the level of cAMP using an HTR-FRET assay. NCI-H716 cells were cultured in 96-well plates coated with Matrigel in supplement GlutaMax DMEM high glucose (Gibco, Thermo Fisher Scientific, Waltham, MA, USA), with 10% FBS and penicillin and streptomycin solution. After 24 h, cells were

stimulated with increasing concentrations of test compounds for 1 h at 37 °C in OptiMEM (Gibco, Thermo Fisher Scientific, Waltham, MA, USA) containing 1 mM 3-isobutyl-1-methylxanthine.

2.6. Cell lysates and EphA2 phosphorylation

Cells were seeded in 12-well Falcon® plates (Corning, Corning, NY, USA, #3513) at the concentration of $7x10^4$ cells/mL, in complete medium and incubated overnight at 37 °C. The day after, cell media was removed and a wash with sterile PBS was performed. Then, cell medium without FBS was added and incubated for 2 h at 37 °C. Next, cells were treated with IALCA, LCA or DMSO at proper concentration and incubated for 20 min at 37 °C. Afterward, 10 min stimulation of EphA2 was obtained with ephrin-A1-Fc 0.25 μg/mL.

Then, the cell culture medium was removed, and cells were rinsed with 1 mL/well of sterile iced PBS and solubilized of iced lysis buffer (1% NP-40, 20 mM Tris (pH 8.0), 137 mM NaCl, 10% glycerol, 2 mM EDTA, 1 mM activated sodium orthovanadate, 10 μg/mL aprotinin, and 10 μg/mL leupeptin). Monolayers were scraped and lysates were collected in vials and centrifuged at 2000 x g for 5 min at 4 °C. Supernatants were moved in new test tubes. The protein content was measured with BCA protein assay kit (Thermo Fisher Scientific, Waltham, MA, USA, #23250) following manufacturer's protocol.

EphA2 Tyr-phosphorylation was measured in cell lysates using a DuoSet® IC Human Phospho-EphA2 ELISA Kit (R&D Systems, Minneapolis, MN, USA, #DYC4056) following the manufacturer's protocol. 96-well ELISA Costar® high binding plate (Corning, Corning, NY, USA, #9018) was incubated overnight at room temperature with EphA2 capture antibody diluted in sterile PBS at the proper concentration. After three washes with wash buffer (0.05% Tween-20 in PBS), the plate was treated with blocking buffer (0.05% NaN_3 1% BSA in PBS pH 7.4) and incubated for 1 h at room temperature. Then, five washes of with wash buffer were performed. Next, 100 μL/well of standardized concentration lysates were added and incubated for 2 h at RT. Following 5 washes, 100 μL/well of detection anti-phospho-tyrosine-HRP (1:1800 in IC14 Diluent) were added and incubated for 2 h at RT. EphA2 phosphorylation was revealed utilizing a standard HRP format with a colorimetric reaction read at 450 nm on Sunrise Tecan plate reader (Tecan, Männedorf, Switzerland), as reported in previous section.

2.7. LDH assay

Non-specific toxicity induced by IALCA on cells was assessed measuring the release of Lactate Dehydrogenase (LDH) into the cell culture medium through the CytoTox 96® non-radioactive cytotoxicity assay (Promega, Madison, WI, USA, #G1780).

Briefly, 100 μL/well of 10^5 cells/mL were seeded in 96-well Falcon® plates (Corning, Corning, NY, USA, #353072) and incubated overnight at 37°C. The next day, cell media was removed and, following a wash with sterile PBS, 90 μL/well of fresh medium without FBS were added. Following two hours of incubation at 37°C, cells were treated with IALCA at proper concentrations, DMSO 0.5% or lysis solution (Triton X-100). After 2 h of incubation, the culture medium was collected and centrifugated at 500 rcf for 30 min to obtain a cell free supernatant. Supernatants were added in a new 96-well Falcon® plate. Then, CytoTox 96® reagent were added and incubated in a dark place for 40 min. The enzymatic activity turns iodonitrotetrazolium violet (INT) into red formazan. Next, stop solution were added and the intensity of coloration observed, which is proportional to the number of lysed cells, was quantified at 492 nm using Sunrise Tecan plate reader (Tecan, Männedorf, Switzerland). Results were expressed as the percentage of absorbance relative to cells treated with lysis solution.

2.8. MTT assay

Cell viability modulation was assessed using MTT assays. Living cells mediate the conversion of MTT (3-[4,5-dimethylthiazol-2-yl]-2,5 diphenyl tetrazolium bromide) into formazan crystals (purple), due to their mitochondrial activity. The intensity of purple coloration from solubilized crystals is related to the number of viable cells.

Briefly, 90 μL/well of a 10^4 cells/mL PC3 cells suspension were seeded in 96-well Falcon® plates (Corning, Corning, NY, USA, #353072) and incubated overnight at 37 °C. Then, IALCA or UniPR1466 or DMSO were added at proper concentrations and incubated for 24 and 48 h at 37 °C. Control was performed at T_0 with DMSO treatment only. Next, cell media was removed and 100 μL/well of MTT solution (1 mg/mL in complete medium) was added and incubated for 2 h at 37 °C. Afterward, MTT solution was removed and DMSO was added. The plate was read at 550/450 nm via Sunrise Tecan plate reader (Tecan, Männedorf, Switzerland).

2.9. Cell rounding assay

As previously described [14], PC3 cells were seeded in 96-well Falcon® plates (Corning, Corning, NY, USA, #353072) at a concentration of 2.5 x 10^4 cells/mL, 100 μl/well, and incubated overnight at 37°C. The following day, cells were rinsed with DPBS w/Ca and Mg (Corning, Corning, NY, USA, #21030CV) and starved overnight in FBS free medium. Next, cells were incubated with IALCA or vehicle (DMSO 0.3%) for 10 min before stimulation with ephrin-A1-Fc 0.5 μg/mL or Fc fragment 0.25 μg/mL for 30 min. Pictures of cells from the same field were taken before (T_0) and after the treatments (T_{40}) on the inverted microscope Leica Dmi1 (Leica Camera, Wetzlar, Germany) at 2.5X magnification. The shape descriptor of circularity was calculated using ImageJ software.

2.10. Molecular **Modelling**

2.10.1. Protein preparation of Eph receptors

EphA2 and EphB2 proteins were extracted from crystal structures of EphA2-ephrin A1 complex (PDB ID: 3HEI [26]) and EphB2-ephrin B2 complex (PDB ID: 1KGY [27]), respectively. Both proteins were prepared using protein preparation wizard within Maestro, version 14.1.138 (Schrödinger Release 2025–4. Maestro 2025.). The preparation process started with the addition of missing hydrogen atoms (selecting the ionized configuration for Asp, Glu, Lys and Arg residues) followed by optimization of hydrogen bond networks to maximize the number of hydrogen bonds. The protein structures were then minimized with OPLS4 (Schrödinger Release 2025–4. Force Fields 2025., [28]) force field with 0.3 Å RMSD constraint on heavy atoms, after which ephrin ligands and water molecules were removed. IALCA structure was obtained from the public database PubChem in mol2 file format whereas UniPR1466 compound was built and optimized with Maestro. Prior to docking, the compounds were optimized with MacroModel (Schrödinger Release 2025–4. MacroModel 2025.) on default setting; using OPLS4 force field coupled with an implicit water model, and the Polak–Ribiere conjugate gradient method to reach to an energy gradient of 0.05 kj/(mol • Å).

2.10.2. Docking within Eph Receptors

IALCA and UniPR1466 were docked into the prepared EphA2 or EphB2 structures with Glide (Schrödinger Release 2025–4. Glide 2025.), a receptor-ligand docking software implemented in Maestro. Following previous studies [29] docking grids were positioned on the center of mass of the hydrophobic channel of EphA2 or EphB2 structure. Enclosing and bounding boxes dimensions were set to 20 Å and 10 Å on all sides, respectively. The docking protocol was carried out under standard precision mode with flexible ligand sampling and no scaling of vdW radii. The docking results for IALCA in EphA2 revealed two binding modes, A and B, with G_{Scores} and E_{model} values of −5.4 and −34.6 kcal/mol, and −4.9 kcal/mol and −29.9 kcal/mol, respectively. In the case of UniPR1466, docking simulations identified a single binding mode in

both EphA2 and EphB2 receptors resembling binding mode A reported IALCA.

2.10.3. MD simulations of EphA2-IALCA complexes

Before moving on to MD simulations, IALCA was parameterized using the Jaguar package (Schrödinger Release 2025–4. Jaguar pKa 2025.) with the B3LYP-D3 theory and 6–31 g** basis set. The resulting parameters and complexes models were imported into the leap module for preparation within Amber20 (Case DA, et al. Amber 2020 Reference Manual. San Francisco: 2020.) environment. The protein and general Amber forcefield were set to ff19SB and gaff2 model, respectively. The complexes were solvated in an orthogonal box with a size of 12 Å from the protein surface, with dimensions of 84 Å x 75 Å x 73 Å, containing approximately 12,000 TIP3P [30] water molecules, and neutralized with six Na^+ ion. The systems were minimized and equilibrated for 17 ns under NVT and NPT ensembles, with a gradual temperature increase from 10.0 to 300.0 K and decreasing restrain on both the protein and ligand. The SHAKE algorithm was utilized to constrain covalent bonds involving hydrogen atoms, while long-range electrostatic interactions were treated with particle-mesh of Ewald's summation method [31] with a 10 Å cut-off. The production phase was performed for 200 ns under the NVT ensemble. Each binding pose was submitted to three independent MD simulations. Following simulation completion, analyses including root-mean-square deviation (RMSD), distance between carbon atom of IALCA's carboxylic group and Arg103/Arg159 residues and the key movements of the systems (i.e., essential dynamics) were calculated using the CPPTRAJ module implemented in AMBER [32].

2.10.4. Human ASBT preparation and docking

The apical sodium-dependent BA transporter (ASBT, also known as SLC10A2) protein structure was built by homology modeling using PRIME software [33] implemented within the "Biologics" suite of Schrödinger (Schrödinger Release 2025–4). The human ASBT sequence was obtained from the UniProt database (Accession code: Q12908). A search in the PDB database by PRIME pointed at a bacterial homologue (from Neisseria meningitidis) of hASBT (PDB ID: 3ZUY) in complex with taurocholic acid [34] as the best template structure (sequence similarity = 46%; sequence identity = 24%) for comparative modelling. The same search performed with SWISS-MODEL identified the same structure as reference template. PRIME was thus applied for hASBT model building using default parameters. Taurocholic acid (modelled in its anionic form) was thus manually docked on the model of hASBT after careful 3D-alignment on the X-ray structure of the bacterial homologue. The resulting hASBT-taurocholate complex was then prepared using the same protocol applied for EphA2 and EphB2 and employed to perform docking simulations with Glide software. Compound minimization and docking processes were carried out with the same procedure described above with the docking grid positioned on the superimposed taurocholic acid applying hydrogen bond restraints to engage Asn10 and Asn266 in hASBT.

2.10.5. Data calculations and Statistical analyses

Data were collected and analyzed on Microsoft Excel software (Microsoft, Redmond, WA, USA). Charts, calculations and statistical analyses were performed on GraphPad Prism 9.5.1 (GraphPad Software Inc., La Jolla, CA, USA).

3. Results

3.1. Stereochemical characterization of 3α-hydroxy-5β-cholan-24-oic acid (isoalloLCA, IALCA).

IALCA possesses a peculiar stereochemistry at position 5 (Fig. 2), with the hydrogen atom emerging from the tertiary carbon being axial and associated with an alpha configuration (5α). This stereochemical arrangement determines a *trans*-junction between ring A and ring B and a straight shape to the steroid (i.e., androstane) nucleus. In LCA, the corresponding hydrogen is equatorial (5β configuration), leading to a *cis*-junction between ring A and B and therefore to a bent shape to the steroid substructure. Stereochemistry at the 3-position is also an element of geometrical diversity, with IALCA having a 3β-hydroxy group, and LCA a 3α-hydroxy group.

Given the paucity of experimental structural data for IALCA [35,36], we set out to characterize by NMR spectroscopy the commercially available compound used here. The crowded aliphatic region of the spectrum does not allow a direct *J*-analysis coupled to the chemical shift, impeding a straightforward attribution of signals by simple mono-dimensional NMR spectroscopy. By means of ^{1}H-COSY experiment, we were able to isolate the resonance of the axial H-5 proton (supporting material 1 at https://doi.org/10.5281/zenodo.17979717), allowing us to observe a clear NOE contact between the axial H-5 proton and the axial H-3 proton by a ^{1}H-NOESY experiment (Fig. 3). This spectroscopic evidence demonstrates the absolute configuration at C-5, and the *trans*-junction between ring A and ring B in IALCA.

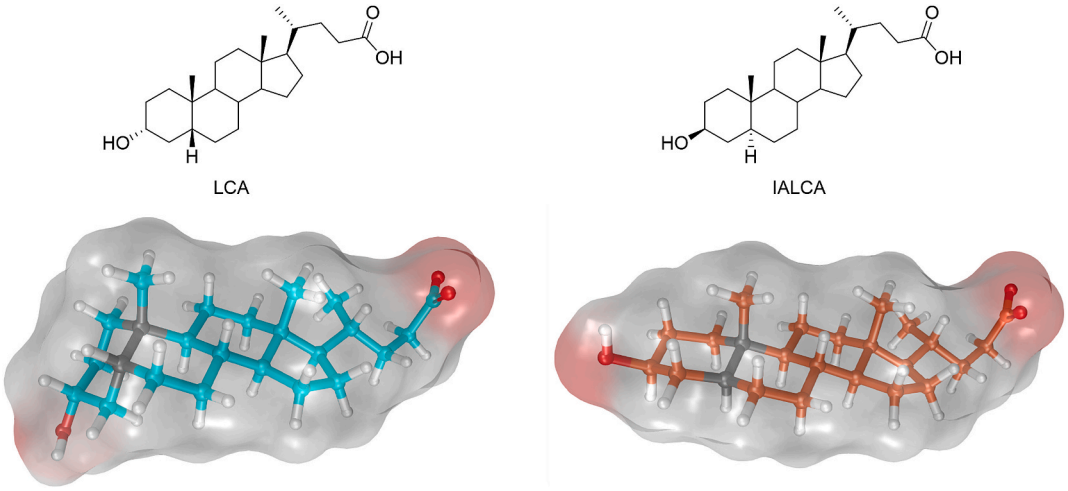


Fig. 2. LCA vs IALCA three-dimensional shape. LCA carbon atoms are colored in cyan except for those involved in *cis*-junction (colored in gray) between ring A and B of the gonane ring. IALCA carbon atoms are colored in orange except for those involved in the *trans*-junction (colored in gray) between ring A and B of the gonane ring. Van der Waals surfaces are also represented (in gray) to display the different shape of the two compounds.

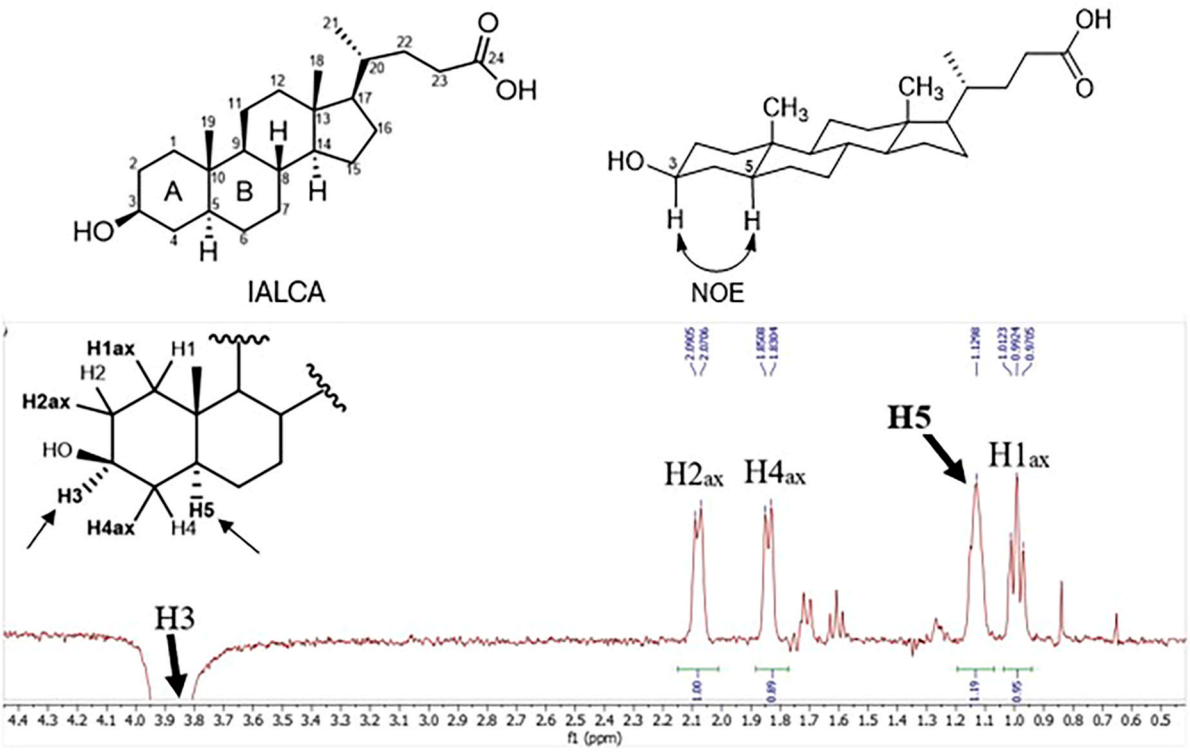


Fig. 3. NMR analysis for IALCA. To identify the H-5 proton, we performed a one-dimensional NOESY experiment, selectively irradiating H-3 at 3.88 ppm. Four NOE interactions were observed with protons at 2.08, 1.84, 1.13, and 0.99 ppm respectively. Analysis of the two-dimensional H-H COSY spectrum revealed that the signals at 2,08 ppm and 1.84 ppm show COSY correlations with H-3. These protons were therefore assigned to axial H-2 and axial H-4, an assignment further supported by the HSQC spectrum. Additionally, the H-H COSY spectrum shows that H-2 correlates with the signal at 0.99 ppm, the resonance assigned to axial H-1. The remaining signal observed in the 1D NOESY experiment at 1.13 ppm is therefore attributed to H-5. This assignment was subsequently confirmed through H-H COSY analysis of the H-4 signal, which correlates with the signal at 1.13 ppm, as well as by other two-dimensional spectra that enabled the complete assignment of all proton and carbon signals. Overall, the strong NOE contact observed between H-3 and H-5 ultimately prove the *trans*-junction of the A and B ring.

3.2. Binding prediction for IALCA at the EphA2 receptor

We evaluated whether IALCA could recognize the ligand binding domain (LBD) of EphA2 by docking and molecular dynamics (MD) simulations. Docking results by Glide software proposed two alternative poses featuring a similar docking score (see Methods) in which IALCA

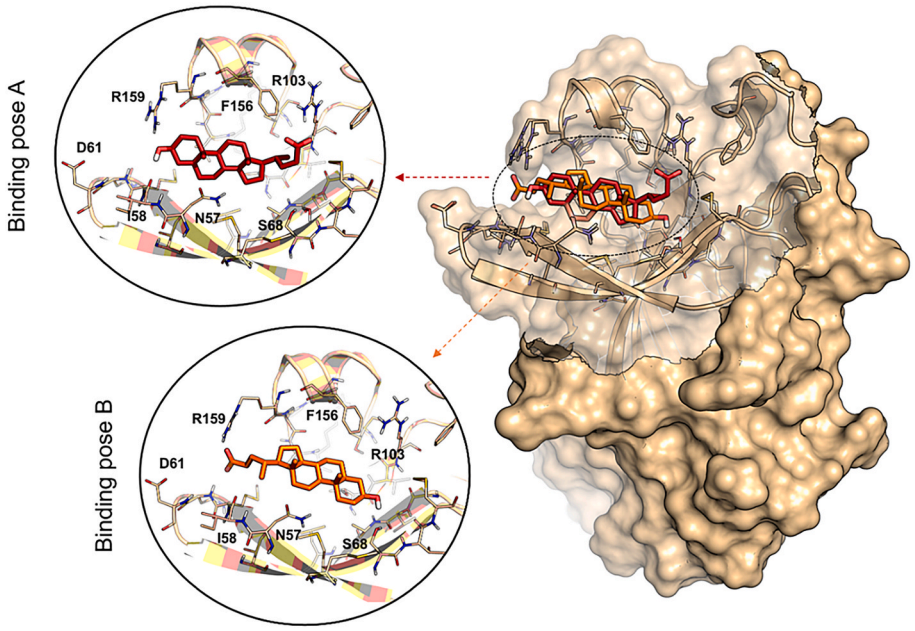


Fig. 4. Proposed binding modes for IALCA within the ligand binding domain (LBD) EphA2 receptor by docking simulations. In evidence in the circle spots EphA2 residues surrounding IALCA, with Arg103 forming a salt bridge with IALCA carboxylate group in binding pose A and with Arg159 interacting with the same functional group of IALCA in binding pose B.

may effectively bind the central hydrophobic channel of the LBD, deputed to the recognition of the G-H loop of ephrin-A1. The first binding mode resembles the one reported for 3β-hydroxy-Δ^5-cholenic acid with the A ring pointing toward with Ile58 and the carboxylate group engaging a salt bridge with Arg103 of EphA2 [37], while the second seems more consistent to what reported later for LCA, in which the carboxylate group of IALCA interacts with Arg159 [38]. To evaluate the proposed binding modes, a set of 3 x 200-ns MD simulations were carried out, starting from the structures displayed in Fig. 4.

In the case of binding pose A, a stable binding mode was observed in two of the three performed MD replicas. In these trajectories, the steroidal core of IALCA stably oscillated around its starting position for the whole duration of the simulation, while the carboxylate group was able to form a salt bridge with Arg103. The time series of the root mean-squared deviation (RMSD) of the ligand as well as of the distance between carboxylate carbon of IALCA and the guanidine carbon of Arg103 confirmed this analysis (Fig. 5, upper panels). In the case of binding pose B, we could not observe a stable arrangement of the ligand, which experienced significant change in its position already in the early stage of the production phase of the MD simulations, as shown by the RMSD time series (Fig. 5, lower panels). Notably, in one of the replicates (#3), IALCA spontaneously left binding pose B, and it assumed an arrangement superimposable to binding mode A undertaking interaction with Arg103 after few nanoseconds of molecular dynamics and oscillated around this pose for the rest of the simulation. Essential dynamics analysis of the MD trajectories, summarizing the movements of IALCA during simulations in the different replicas, is reported in supporting material 2 at https://doi.org/10.5281/zenodo.17979717.

3.3. Pharmacological characterization of IALCA on the Eph-ephrin system

The results of the MD simulations, suggesting the presence of at least one stable binding mode for IALCA at EphA2-LBD, prompted us to verify our hypothesis on the actual ability of IALCA to interfere with binding of ephrin-A1 to EphA2. Therefore, we carried out displacement assays using increasing concentrations of IALCA, ranging from 1.56 μM to 50 μM, in the presence of biotinylated ephrin-A1-Fc at a concentration corresponding to its K_D value (Fig. 6A). IALCA was able to prevent ephrin-A1-Fc binding to EphA2-Fc in a concentration-dependent manner, with a half maximal inhibitory concentration (IC_{50}) value of 5.9 μM. Notably, IALCA was ten times more potent than LCA, with an IC_{50} of 57 μM, although with a steeper concentration–response curve compared to LCA.

We next aimed to calculate Hill slope by charting saturation curves of different concentrations of biotinylated ephrin-A1-Fc on immobilized EphA2-Fc receptor in presence of IALCA in a concentration range between 3.125 μM and 12.5 μM (Fig. 6B). IALCA showed an approximated K_i value in the low micromolar range (6.5 μM) but the very steep curve is also reflected in this assay, making us unable to properly calculate the Hill coefficient.

Afterward, we investigated the selectivity of IALCA for Eph receptors. Hence, we performed displacement assays against biotinylated ephrin-A1-Fc binding to eight EphAs and biotinylated ephrin-B1-Fc binding to four EphBs (Fig. 6C). Three concentrations of IALCA were tested, ranging from 1 to 10 μM. IALCA showed to discriminate between EphAs and EphBs subclasses as being able to significantly affect only binding of ephrin-A1-Fc to EphA receptors (Table 1). The current selectivity profile of IALCA on the Eph receptors is very different from that of LCA which interferes with ephrin binding to all the cloned Eph

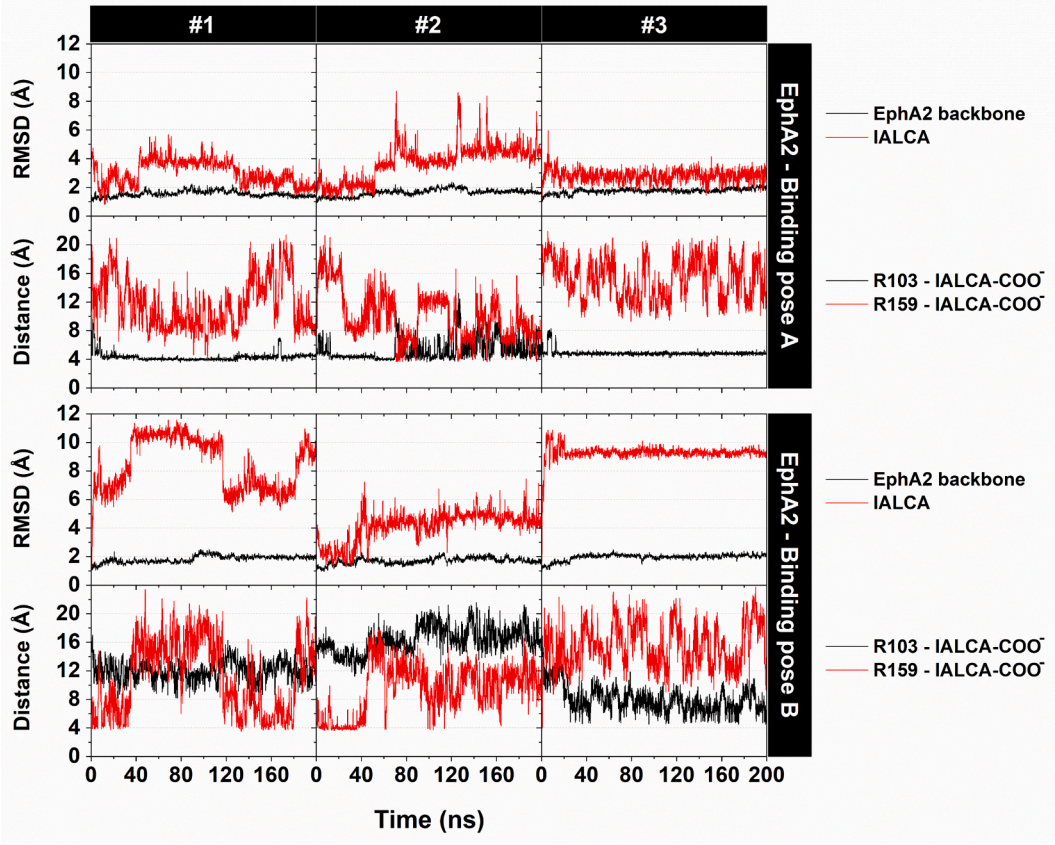


Fig. 5. Time series of the RMSD calculated for IALCA heavy atoms and EphA2 backbone in a set of 3 independent MD simulations started from binding pose A and B reported in Fig. 2. The key distance between the carbon atom of the carboxylate group of IALCA and the carbon atom of the guanidine group of Arg103 and Arg159.

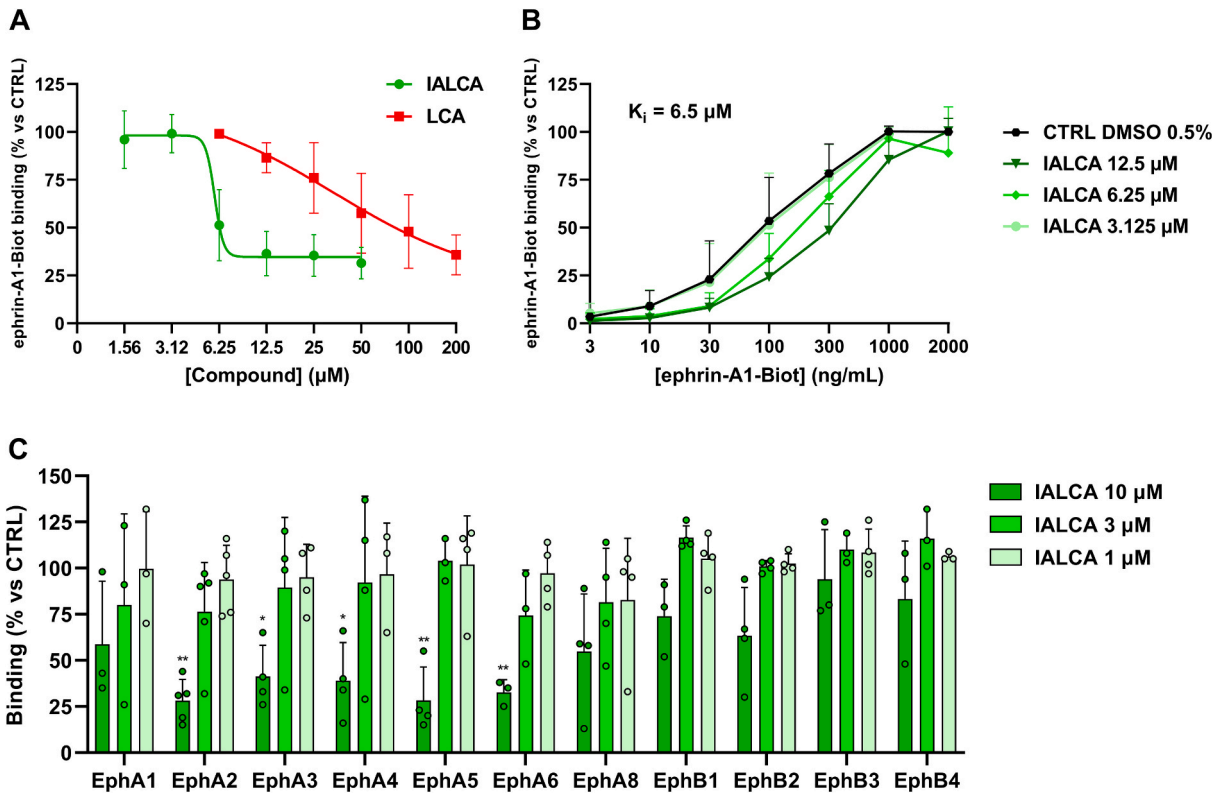


Fig. 6. (A) Binding curves for IALCA (IC_{50} = 5.9 μM) and LCA (IC_{50} = 57 μM) displacing ephrin-A1 from EphA2. (B) Binding of biotinylated ephrin-A1-Fc to EphA2-Fc in the presence of increasing concentrations of IALCA. (C) Effect of IALCA on the binding of biotinylated ephrin-A1-Fc with EphAs and biotinylated ephrin-B1-Fc with EphBs. Ligands were used at their K_D values. Comparisons were performed vs Control DMSO 0.5% which arbitrarily represents 100% of binding (data not shown). Reported data are the means of at least three independent experiments ± standard deviation. Non-linear regression, IC_{50}/K_i calculations, and statistical analyses using 2way ANOVA multiple comparisons followed by Tukey's post-test were performed on GraphPad Prism Software (*p < 0.05, **p < 0.01 vs Control DMSO 0.5%).

Table 1
IC_{50} values (95%-c.l.) of IALCA and UniPR1466 on different members of Eph family of receptors.

Receptor	IC_{50} [μM] IALCA	Receptor	IC_{50} [μM] UniPR1466
EphA1	>10	EphA1	6.3 (2.6 – 16)
EphA2	6.4 (4.1 – 10)	EphA2	5.9 (4.0 – 8.8)
EphA3	10.3 (5.4 – 22)	EphA3	11 (5.8 – 20)
EphA4	10.4 (4.5 – 30)	EphA4	9.1 (4.7 – 18)
EphA5	9.2 (4.7 – 21)	EphA5	5.9 (3.4 – 10)
EphA6	7.1 (4.4 – 12)	EphA6	7.8 (3.5 – 20)
EphA8	>10	EphA8	4.6 (2.5 – 8.3)
EphB1	Inactive	EphB1	13 (7.9 – 23)
EphB2	Inactive	EphB2	12 (7.5 – 18)
EphB3	Inactive	EphB3	>30
EphB4	Inactive	EphB4	15 (6.3 – 41)

receptor subtypes with a similar IC_{50} value.

3.4. Selectivity of IALCA versus bile acid targets

The classical receptors for BAs include farnesoid X receptor (FXR), a nuclear hormone receptor highly expressed in the liver and intestine mediating the expression of specific genes involved in BA synthesis and homeostasis, and the membrane-bound G protein-coupled BA receptor 1 (GPBAR-1, also known as TGR5), primarily expressed in the gut and in the brown adipose tissue whose activation initiates the non-genomic signaling pathways of BAs. Available structural and SAR information indicates that a 3α, 5β configurations favor binding and activation of both FXR and TGR5 [39–41]. We thus speculated that, due to its 3 β, 5α stereochemistry, IALCA would not bind these two receptors. Hence, the activity of IALCA on FXR and TGR5 was evaluated by a luminescence (EnVision microplate analyzer) and HTR-FRET assay, respectively. IALCA failed to activate both receptors at all tested concentrations (up to 50 μM). In similar conditions, LCA activates FXR and TGR5 with an EC_{50} of 25 μM [42] and 0.73 μM [43], respectively. We extended our analysis to other nuclear receptors of interest in the context of steroidal compounds biology such as pregnane X receptor (PXR) and liver X receptor (LXR). Also in this context, IALCA resulted inactive up to 50 μM when tested on both.

3.5. Activity of IALCA in cellular assays

Then, we pursued further investigations with functional assays in human prostate adenocarcinoma (PC3) cells. This represents an ideal model for studying EphA2 biology because of its *i.* robust and consistent EphA2 overexpression, *ii.* functional dependence on EphA2 signaling for key malignant phenotypes, *iii.* translational relevance in the context of cancer therapy [44]. First, we investigated the non-specific cytotoxicity of IALCA through Lactate Dehydrogenase (LDH) quantification. As shown in Fig. 7A, the incubation of IALCA for two hours did not cause a significant LDH release in the cellular medium up to 30 μM, highlighting the absence of non-specific damage. According to these data, we induced EphA2 tyrosine phosphorylation with 0.25 μg/mL ephrin-A1-Fc and tested the phosphorylation levels of EphA2 after treatment with IALCA. EphA2 phosphorylation was significantly reduced in PC3 cell line treated with IALCA (Fig. 7B) and it was roughly 3-fold more potent than LCA (IC_{50} = 18 μM vs IC_{50} = 48 μM, respectively).

As previously established, ephrin-A1 is able to regulate cell rounding and retraction fiber formation upon EphA2 activation [45]. To evaluate if IALCA may exert functional antagonism, we carried out cell rounding

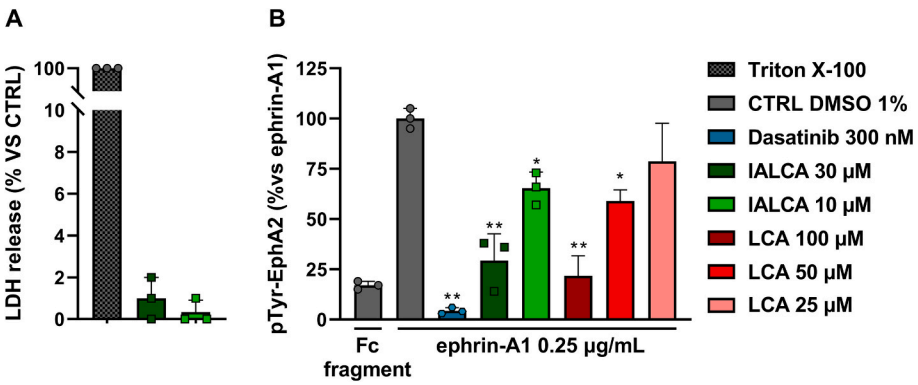


Fig. 7. (A) Lactate Dehydrogenase (LDH) released from PC3 cells incubated for two hours with IALCA. 0.3% DMSO (not shown) and Triton X-100 (CTRL) were considered as 0% and 100%, respectively. (B) Relative EphA2 phosphorylation in the presence of different concentrations of IALCA, LCA and Dasatinib. Cells were treated for 20 min with 1% DMSO or compounds, stimulated with ephrin-A1-Fc for 10 min before proceeding with lysis. Data are normalized on stimulated treatment (1% DMSO + 0.25 µg/mL ephrin-A1-Fc), which arbitrarily represented 100% of EphA2 phosphorylation. Data are the means of at least three independent experiments ± st.dev. Statistical analysis was performed on GraphPad Prism software using 2-ways ANOVA multiple comparisons followed by Tukey's post-test (*$p < 0.05$, **$p < 0.01$ vs DMSO 1% + 0.25 µg/mL ephrin-A1-Fc).

assays in PC3 cells. As reported in Fig. 8, IALCA was able to completely revert the effect of ephrin-A1-Fc at 30 µM, whilst no differences were observed at 10 µM. Conversely, IALCA at 30 µM alone did not affect cell morphology compared to control cells treated with Fc fragment (equimolar to ephrin-A1-Fc).

4. IALCA as a template structure to design Eph-ephrin antagonists

Gut microbiota hydrolyzes host-produced taurine/glycine conjugates releasing free BAs thanks to conjugated BA hydrolase (CBAH). The same CBAH enzyme exhibits N-acyltransferase activity, re-conjugating these BAs with free amino acids abundant in the intestinal lumen thus producing MABAs [46]. The most intriguing non-taurine/non-glycine amino acid conjugates of bile acids are those based on L-Trp. Cholic

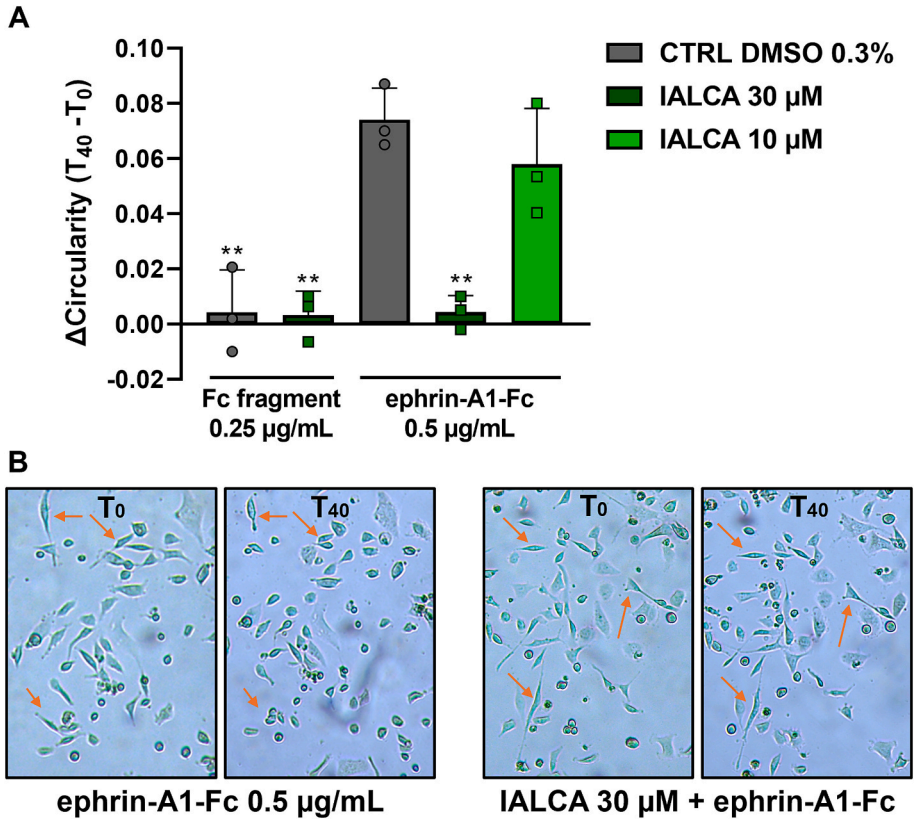


Fig. 8. (A) PC3 cells circularity variation (roundness shape descriptor) upon treatment with ephrin-A1-Fc and IALCA at different concentrations. Cells were treated with IALCA (30 and 10 µM) or DMSO 0.3% and incubated for 10 min at 37°C. Next, cells were treated with ephrin-A1-Fc 0.5 µg/mL or Fc fragment 0.25 µg/mL and incubated for 30 min at 37°C. T_0 and T_{40} pictures were taken and analyzed with ImageJ software. Data are the means of at least three different wells in three independent experiments ± st.dev. One-way ANOVA followed by Tukey's post-test was performed on GraphPad Prism software (**$p < 0.01$ vs CTRL DMSO 0.3% + 0.5 µg/mL ephrin-A1-Fc). (B) Representative pictures of PC3 cells before and after treatment with ephrin-A1-Fc alone or in combination with IALCA 30 µM.

acid–tryptophan (Trp-CA) conjugate has recently emerged as new signaling molecule contributing to glucose homeostasis [47]. Also, in the context of the Eph-ephrin system, L-Trp conjugates of bile acids always displayed a consistent and reproducible antagonistic activity, suggesting that conjugation of IALCA with L-Trp may provide a new compound featuring a pharmacological activity on Eph receptors.

Visual analysis of the EphA2-IALCA complex (binding mode A) suggested that the region of the LBD beyond Arg103, delimited by the aromatic side chain of Phe108, could be occupied by suitable aromatic structures, properly connected to the terminal carboxylic acid of IALCA. As previously reported for 3β-hydroxy-Δ^5-cholenic acid (Castelli et al, 2015), conjugation with aromatic α-amino acids appeared particularly promising. Docking simulations supported this hypothesis (Fig. 9), prompting us to synthesize and pharmacologically characterize the L-Trp conjugate of IALCA, UniPR1466, by applying the synthetic procedure reported in supporting material 3 at https://doi.org/10.5281/zenodo.17979717, as previously applied to the synthesis of amino-acid conjugates of 3β-hydroxy-Δ5-cholenic acid [29].

We thus performed displacement assays with increasing concentrations of UniPR1466, ranging from 1.6 μM to 50 μM, in the presence of biotinylated ephrin-A1-Fc at its K_D value (Fig. 10A). UniPR1466 was active in the ELISA-like binding assay where it showed an IC_{50} value of 4.1 μM, comparable to that of IALCA. Nevertheless, our data showed that UniPR1466 is more effective than IALCA in the displacement activity as being able to completely inhibit ephrin-A1-EphA2-Fc binding. Conversely, in our experimental setting IALCA was able to only reach the 75% of ephrin-A1-EphA2-Fc binding inhibition. This difference may reflect a better solubility of UniPR1466 in the ELISA binding buffer in comparison to IALCA. Displacement assays were repeated by incubating IALCA or UniPR1466 for 1 h and washing the wells before adding ephrin-A1-Fc. Under, these conditions, the compounds were unable to reduce ephrin-A1-Fc binding suggesting a reversible binding (supporting material 4 at https://doi.org/10.5281/zenodo.17979717).

For a better assessment of the affinity of the L-Trp conjugate for EphA2, we built saturation curves of different concentrations of biotinylated ephrin-A1-Fc in presence of UniPR1466 in a concentration range between 12.5 μM and 50 μM (Fig. 10B). UniPR1466 showed a K_i value in the low micromolar range (3.6 μM), slightly lower than that displayed by IALCA ($K_i = 6.5$ μM). This analysis gave a Hill coefficient of 1.2 which suggests a competitive antagonism for this compound (supporting material 4 at https://doi.org/10.5281/zenodo.17979717).

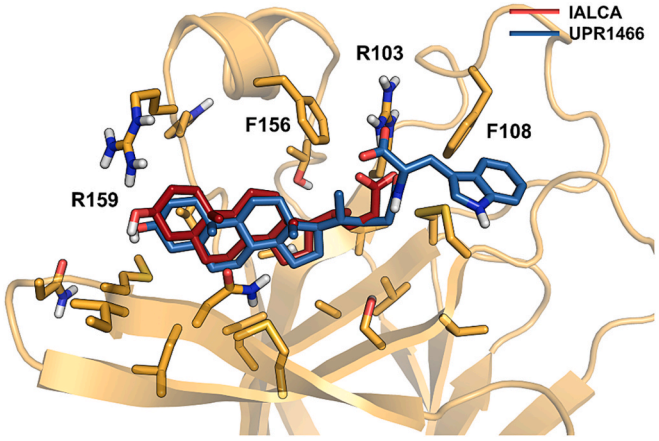


Fig. 9. Proposed binding mode for UniPR1466 (blue carbon atoms) within the ligand binding domain (LBD) of EphA2 (gold carbon atoms) superposed to the structure of IALCA (brown carbon atoms). Both compounds occupy the hydrophobic channel of the LBD thanks to their common steroidal structure and undertake polar interactions with Arg103 by means of their terminal carboxylate group. The indole ring of UniPR1466 undertakes additional interactions with the phenyl ring of Phe108 in a region of the LBD which is conserved among all the cloned Eph receptors.

We thus evaluated the activity of UniPR1466 on other Eph receptors. Hence, we performed displacement assays against biotinylated ephrin-A1-Fc binding to seven EphAs and biotinylated ephrin-B1-Fc binding to four EphBs (Fig. 10C). Differently from IALCA, UniPR1466 was able to dose-dependently prevent either binding of ephrin-A1 or ephrin-B1 to EphA1-EphA8 and EphB1-B4 respectively, suggesting that L-Trp moiety of UniPR1466 targets a key subpocket likely present in all the Eph receptors allowing to improve affinity.

Superposition of UniPR1466 docked in the LBD of EphA2 and EphB2 on the X-ray coordinates of EphA2-ephrin-A1 and EphB2-ephrin-B1 complexes shows that the L-Trp moiety of the titled compound occupies the same space of a key Phe residue belonging to the −x-x-ϕ binding motif of the ephrins (supporting material 5 at https://doi.org/10.5281/zenodo.17979717). This ϕ–x–x–ϕ motif (where "x" represents any amino acid, and "ϕ" typically a Phe residue) is a critical conserved sequence found in the ephrin ligands (both ephrin-A and ephrin-B subclasses) that is essential for their high-affinity binding to the Eph receptor tyrosine kinases [48].

Next, we carried out functional assays to evaluate UniPR1466 activity in vitro. First, we examined the non-specific cytotoxicity of UniPR1466 through released LDH quantification. As shown in Fig. 11A, similarly to IALCA, the incubation of UniPR1466 for two hours did not cause a significant LDH release in the cellular medium.

Then, we induced EphA2 tyrosine phosphorylation upon stimulation with 0.25 μg/mL ephrin-A1-Fc. Phosphorylation levels of EphA2 were evaluated after treatment with UniPR1466 used at three different concentrations (Fig. 11B). EphA2 phosphorylation was significantly reduced in PC3 cell line treated with UniPR1466 (IC_{50} = 10 μM). However, no significant differences were observed compared to IALCA.

Lastly, we tested whether IALCA and UniPR1466 could interfere with PC3 cell proliferation. Hence, we conducted MTT assays at three treatment conditions (IALCA/UniPR1466 3–30 μM) at 24 and 48 h. As shown in Fig. 11C, 48 h of treatment with IALCA show no effects at all up to 10 μM and a minor reduction of cell proliferation at 30 μM. On the other hand, UniPR1466 30 μM significantly reduced cell proliferation both at 24 and 48 h, showing a significant cytostatic effect (Fig. 11D).

While the active transport in the bile of IALCA and MABA derivatives still needs to be experimentally assessed, we have recently observed that UniPR1331 (Fig. 1), an L-Trp conjugate similar to UniPR1466, experienced a significant entero-hepatic circulation and accumulated in the bile fluid when orally administered in mice [49]. *In vitro* investigations performed by our research group (supporting material 4 at https://doi.org/10.5281/zenodo.17979717) showed that UniPR1331 interacted with human apical bile acid transporter (hASBT) expressed in CHO cells in a concentration-dependent manner, confirming that this compound is transported by this BA carrier. Considering the structural similarity between UniPR1331 and UniPR1466 (Tanimoto 2D similarity = 0.838) and between UniPR1331 and IALCA (Tanimoto 2D similarity = 0.643), we speculate that also UniPR1466 and IALCA can interact with the ASBT experiencing bile fluid accumulation. To support this hypothesis, we computationally evaluated whether UniPR1466 and IALCA could interact with hASBT applying an in-silico protocol similar to that reported by Temprano and colleagues [18]. In brief, docking studies show that IALCA and UniPR1466 can assume a binding mode in hASBT resembling that of UniPR1331 and taurocholic acid (TCA), employed as additional control compound (Fig. 12). Moreover, IALCA and UniPR1466 display interaction energies with ASBT (i.e., Gscore) comparable to those of the control compounds.

5. Discussion

BAs (including their amino acid conjugates) are very well known for their role in lipid digestion [50], and they are now recognized as key signaling molecules regulating metabolism and energy homeostasis as well as inflammatory responses in humans [51,52] acting at the interface between host metabolism, immunity, and gut microbiota [53].

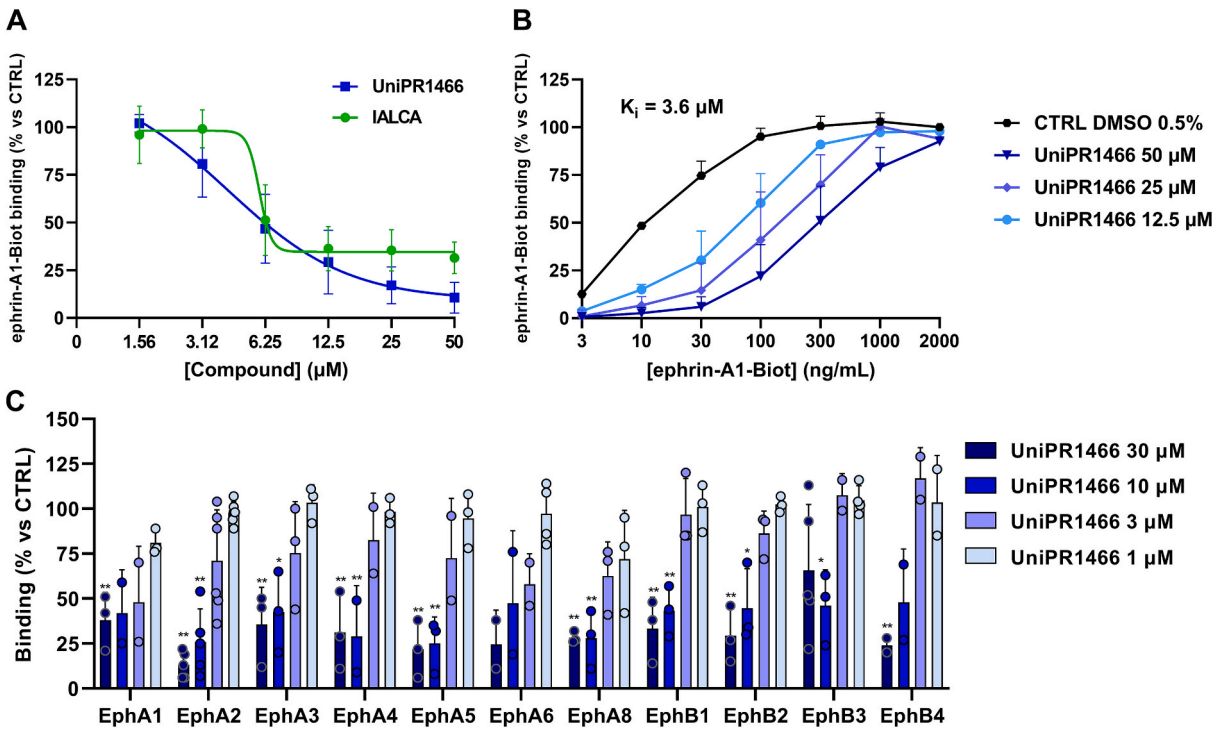


Fig. 10. (A) Binding curves for IALCA (IC_{50} = 5.9 μM) and UniPR1466 (IC_{50} = 4.1 μM) displacing ephrin-A1 from EphA2. (B) Binding of biotinylated ephrin-A1-Fc to EphA2-Fc in the presence of increasing concentrations of UniPR1466. (C) Displacement activity of UniPR1466 on the association of biotinylated ephrin-A1-Fc with EphAs and biotinylated ephrin-B1-Fc with EphBs. Ligands were used at their K_D values. Comparisons were performed vs Control DMSO 0.5% which arbitrarily represents 100% of binding (data not shown). Reported data are the means of at least two independent experiments ± standard deviation. Non-linear regression, IC_{50}/K_i calculations, and statistical analyses using 2-way ANOVA multiple comparisons followed by Tukey's post-test were performed on GraphPad Prism Software (*$p < 0.05$, **$p < 0.01$ vs Control DMSO 0.5%).

A central pathway of BA signaling involves the nuclear receptor FXR, which regulates genes involved in BA synthesis, transport, and detoxification, creating a negative feedback loop that maintains BA homeostasis. BAs also signal through the G protein–coupled BA receptor TGR5. Activation of TGR5 leads to effects such as enhanced energy expenditure, stimulation of glucagon-like peptide-1 (GLP-1) secretion from enteroendocrine cells, and anti-inflammatory actions in macrophages [54,55]. Additional receptors modulated by BAs include PXR, VDR and Eph receptors, further expanding BA signaling roles,

Our research group identified LCA, a dual TGR5 and FXR agonist, as a pan-Eph/ephrin competitive and reversible antagonist. In an extension of our work, we discovered new Eph/ephrin inhibitors within natural BAs, LCA-derivatives and synthetic FXR agonists, suggesting that the structural requirements to bind Eph receptors, TGR5 and FXR might be similar. [14,17,56,57].

Herein, we characterized the biochemical activity of a rare secondary BA structurally related to LCA, known as IALCA. IALCA is significantly abundant in centenarians and has been shown to protect gut from inflammation [20,23,24]. IALCA is a signature metabolite of a specialized subset of gut bacteria able to generate a transient 3-oxo-Δ^4-intermediate *via* multistep modifications of the primary BA chenodeoxycholic acid. The biological activity of IALCA is a straightforward example about how minor microbial metabolic pathways can affect host physiology.

Our investigation reveals, for the first time, a clear and concentration-dependent activity of IALCA on the EphA2/ephrin-A1 signaling axis. Importantly, IALCA displaces ephrin-A1 from EphA2 receptor with higher potency than its LCA stereoisomer. However, the unusual slope of the concentration–response curve observed for IALCA in the EphA2-ephrinA1 displacement assay makes uncertain the nature of its antagonism. As artifacts resulting from irreversible binding of IALCA can be ruled out based on the reversibility assay, and a Hill coefficient of 1.2 was found for the L-Trp conjugate of IALCA (UniPR1466), we speculate that this bile acid also acts as a competitive antagonist. However, further biophysical studies (e.g. FCCS-PIE, NMR, SPR) are needing to definitively resolve the issue.

Functional assays performed on PC3 cells (a well-established model of EphA2 overexpression) show that IALCA dose-dependently reduces EphA2 tyrosine-phosphorylation induced by ephrin-A1, in absence of non-specific toxicity. Moreover, IALCA completely abolishes ephrin-A1-mediated cell rounding, confirming the ability of this compound to engage EphA2 in cells. When tested on all Eph-ephrin pairs of −A and −B classes, IALCA is more selective than LCA as it preferentially binds to EphAs, thus sparing EphB receptors.

This last observation could offer an interesting explanation about the detrimental effect of LCA on intestinal homeostasis [58] in opposition to the beneficial effects of IALCA. The opposing biological effects of LCA and its IALCA isomer may rely on their differential engagement with the Eph/ephrin signaling system. While both act as EphA2 receptor antagonists, LCA additionally interferes with ephrin-B-mediated pathways, potentially disrupting intestinal stem cell niches reliant on EphB/ephrin-B signaling [59]. Conversely, IALCA could specifically counteract inflammation-driven epithelial permeability mediated by EphA2, while preserving stem cell compartment integrity [60]. This distinct receptor targeting profile provides a plausible mechanistic base for IALCA observed anti-inflammatory and tissue-protective effects, contrasting with LCA's documented pro-inflammatory and pro-carcinogenic activities [61]. It is worth noting that concentrations of IALCA in *in vitro* experiments can also be relevant for human health, in particular for centenarians whose median concentration of IALCA is 19.5 μM. Its impact is still relevant on 80-years-old people but almost negligible in younger adults (<55 years old), where IALCA concentrations are fairly low [20].

A brief comparison of selected EphA2-ephrin-A1 inhibitors is

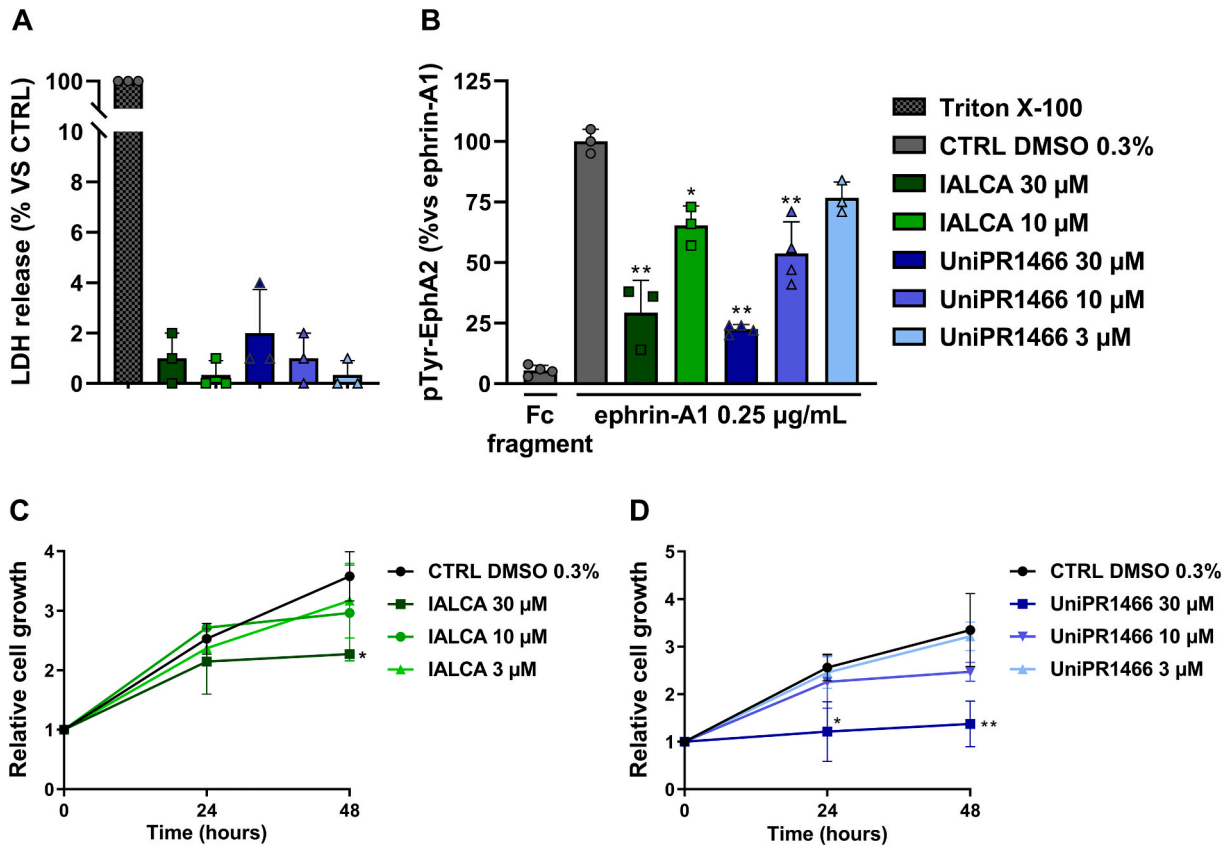


Fig. 11. (A) Lactate Dehydrogenase (LDH) released from PC3 cells incubated for two hours with UniPR1466. 0.3% DMSO (not shown) and Triton X-100 ($CTRL^{+}$) were considered as 0% and 100%, respectively. (B) Relative EphA2 phosphorylation in the presence of different concentrations of IALCA and UniPR1466. Cells were treated for 20 min with 0.3% DMSO or compounds. Next, cells were stimulated with ephrin-A1-Fc for 10 min before proceeding with lysis. Data are normalized on stimulated treatment (0.3% DMSO + 0.25 µg/mL ephrin-A1-Fc), which arbitrarily represented 100% of EphA2 phosphorylation. (C) Relative growth curves of PC3 cells in the presence of IALCA at different concentrations. Separated plates were grown for 24 or 48 h with the compound or DMSO 0.3% and MTT assays were performed. Growth curves are generated by dividing T_X absorbance by T_0 reference absorbance of seeded cells in DMSO 0.3%. (D) Relative growth curve of PC3 cells in the presence of UniPR1466 at different concentrations. Data are the means of at least three independent experiments ± st.dev. Statistical analysis was performed on GraphPad Prism software using 2-ways ANOVA multiple comparisons followed by Tukey's post-test (*$p < 0.05$, **$p < 0.01$ vs (B) 0.3% DMSO + 0.25 µg/mL ephrin-A1-Fc / vs (C/D) CTRL DMSO 0.3%).

summarized in Table 2. IALCA represents the most active secondary BA, being able to engage EphA2 receptor in cell-free assay in the single-digit micromolar range, as opposite to LCA and 3β-hydroxy-Δ^5-cholenic acid which require higher concentration to effectively displace ephrin-A1 from EphA2. IALCA approaches IC_{50} values comparable to those of reference L-Trp conjugates of BA, UniPR126 and UniPR1331, resulting significantly more potent than dual FXR/EphA2 ligands GW4064 and Cilofexor.

Lastly, UniPR1466 demonstrates that structural optimization of IALCA by amino acid conjugation can yield analogs with enhanced potency in *in vitro* functional experiments, suggesting a further development of the class for the potential treatment of inflammatory gut diseases.

6. Declaration of generative AI and AI-assisted technologies in the manuscript preparation process.

During the preparation of this work the authors used "Deepseek 3.2" in order to improve the readability of some sentences. After using this tool, the authors reviewed and edited the content as needed and take full responsibility for the content of the published article.

CRediT authorship contribution statement

Andrea Blesio: Writing – review & editing, Writing – original draft, Visualization, Validation, Methodology, Investigation, Formal analysis, Data curation. **Carmine Giorgio:** Writing – review & editing, Writing – original draft, Validation, Supervision, Methodology, Investigation, Formal analysis, Data curation. **Francesca Romana Ferrari:** Resources, Methodology, Investigation, Formal analysis, Data curation, Conceptualization. **Stefano Sala:** Resources, Methodology, Investigation, Formal analysis, Data curation. **Lisa Flammini:** Investigation, Formal analysis, Data curation. **Ilaria Zanotti:** Writing – review & editing, Writing – original draft, Resources, Methodology, Formal analysis. **Daniela Passeri:** Methodology, Investigation, Formal analysis, Data curation. **Antimo Gioiello:** Methodology, Investigation, Formal analysis, Data curation. **Lorenzo Sarcone:** Visualization, Methodology, Investigation, Formal analysis, Data curation. **Riccardo Castelli:** Writing – review & editing, Writing – original draft. **Kun Karnchanapandh:** Validation, Software, Methodology, Investigation, Formal analysis, Data curation. **Federica Vacondio:** Methodology, Investigation, Formal analysis, Data curation. **Lorenzo Tagliazucchi:** Formal analysis, Data curation. **Laura Scalvini:** Resources, Methodology, Investigation, Formal analysis, Data curation. **Marco Mor:** Software, Funding acquisition. **Alessio Lodola:** Writing – review & editing, Writing – original draft, Visualization, Validation, Supervision, Software, Project administration, Methodology, Investigation, Funding acquisition, Formal analysis, Data curation, Conceptualization. **Massimiliano Tognolini:** Writing – review & editing, Writing – original draft, Validation, Supervision, Project administration, Methodology, Investigation, Funding acquisition, Formal

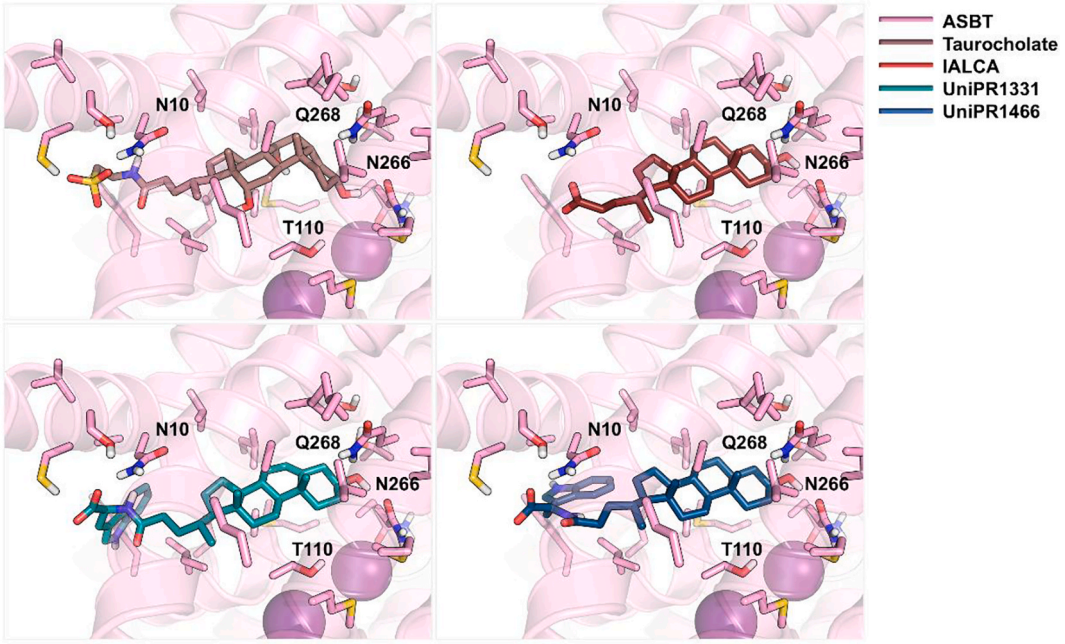


Fig. 12. Binding poses of selected BA (TCA, brown carbon atoms; IALCA, orange carbon atoms) and BA conjugates (UniPR1331, cyan carbon atoms; UniPR1466, blue carbon atoms) within a three-dimensional model of hASBT (pink carbon atoms and cartoons) build by comparative modelling using PRIME (see Methods).

Table 2
IC_{50} values of different compounds in EphA2-ephrin-A1 binding and in PC3 cells Tyr-EphA2 phosphorylation. Data from [14,29,37,62–64].

Compound	EphA2-ephrinA1 displacement IC_{50} [μM]	Inhibition of ephrin-A1 mediated pTyr-EphA2 IC_{50} [μM]
LCA	57	48
UniPR126	2.0	12
3β-hydroxy-Δ^5-cholenic acid	40	NA
UniPR1331	3.5	9.3
IALCA	5.9	18
UniPR1466	4.1	10
GW4064	22	31
Cilofexor	35	>50

analysis, Data curation, Conceptualization.

Funding

This work was supported by Associazione Italiana Ricerca sul Cancro (AIRC IG 22873) to MT. The funder had no role in study design, data collection and analysis, decision to publish, or preparation of manuscript.

This research benefits from the HPC (High Performance Computing) facility of the University of Parma, Italy (https://www.hpc.unipr.it), Regione Emilia-Romagna is kindly acknowledged for supporting FutureData4EU fellowship (to K.K.) at the University of Parma through a MSCA-COFUND action.

Declaration of competing interest

The authors declare that they have no known competing financial interests or personal relationships that could have appeared to influence the work reported in this paper.

Data availability

Chemical characterization, synthesis of the new compound and relative NMR spectra, purity and mass spectrum are available at 10.5281/zenodo.17979717

References

[1] L. Toracchio, M. Carrabotta, C. Mancarella, A. Morrione, K. Scotlandi, EphA2 in cancer: molecular complexity and therapeutic opportunities, Int. J. Mol. Sci. 25 (2024) 12191, https://doi.org/10.3390/ijms252212191.
[2] Y. Wu, Z. Du, J. Mou, X. Qiu, J. Chen, S. Cai, D. Ren, F. Xiao, G. Zhou, C. Yuan, The functions of EphA1 receptor tyrosine kinase in several tumors, Curr. Med. Chem. 30 (2023) 2340–2353, https://doi.org/10.2174/0929867329666220820125638.
[3] A. Arcas, D.G. Wilkinson, M.Á. Nieto, The evolutionary history of ephs and ephrins: toward multicellular organisms, Mol. Biol. Evol. 37 (2020) 379–394, https://doi.org/10.1093/molbev/msz222.
[4] E.B. Pasquale, Eph receptor signaling complexes in the plasma membrane, Trends Biochem. Sci 49 (2024) 1079–1096, https://doi.org/10.1016/j.tibs.2024.10.002.
[5] J.-P. Himanen, M.J. Chumley, M. Lackmann, C. Li, W.A. Barton, P.D. Jeffrey, C. Vearing, D. Geleick, D.A. Feldheim, A.W. Boyd, M. Henkemeyer, D.B. Nikolov, Repelling class discrimination: ephrin-A5 binds to and activates EphB2 receptor signaling, Nat. Neurosci. 7 (2004) 501–509, https://doi.org/10.1038/nn1237.
[6] H. Qin, R. Noberini, X. Huan, J. Shi, E.B. Pasquale, J. Song, Structural characterization of the EphA4-Ephrin-B2 complex reveals new features enabling eph-ephrin binding promiscuity, J. Biol. Chem. 285 (2010) 644–654, https://doi.org/10.1074/jbc.M109.064824.
[7] E.B. Pasquale, Eph-ephrin bidirectional signaling in physiology and disease, Cell 133 (2008) 38–52, https://doi.org/10.1016/j.cell.2008.03.011.
[8] M. Liu, J.G. Charek, R.D. Vicetti Miguel, T.L. Cherpes, Ephrin-Eph signaling: an important regulator of epithelial integrity and barrier function, Tissue Barriers (2025) 2462855, https://doi.org/10.1080/21688370.2025.2462855.
[9] T. Takahashi, A. Shiraishi, J. Murata, S. Matsubara, S. Nakaoka, S. Kirimoto, M. Osawa, Muscarinic receptor M3 contributes to intestinal stem cell maintenance via EphB/ephrin-B signaling, Life Sci. Alliance 4 (2021) e202000962, https://doi.org/10.26508/lsa.202000962.
[10] P. Qiu, D. Li, C. Xiao, F. Xu, X. Chen, Y. Chang, L. Liu, L. Zhang, Q. Zhao, Y. Chen, The Eph/ephrin system symphony of gut inflammation, Pharmacol. Res. 197 (2023) 106976, https://doi.org/10.1016/j.phrs.2023.106976.
[11] M.G. Coulthard, M. Morgan, T.M. Woodruff, T.V. Arumugam, S.M. Taylor, T. C. Carpenter, M. Lackmann, A.W. Boyd, Eph/Ephrin signaling in injury and inflammation, Am. J. Pathol. 181 (2012) 1493–1503, https://doi.org/10.1016/j.ajpath.2012.06.043.
[12] X. Guo, Y. Yang, J. Tang, J. Xiang, Ephs in cancer progression: complexity and context-dependent nature in signaling, angiogenesis and immunity, Cell Commun. Signal 22 (2024) 299, https://doi.org/10.1186/s12964-024-01580-3.
[13] X. Shi, R. Lingerak, C.J. Herting, Y. Ge, S. Kim, P. Toth, W. Wang, B.P. Brown, J. Meiler, K. Sossey-Alaoui, M. Buck, J. Himanen, D. Hambardzumyan, D. B. Nikolov, A.W. Smith, B. Wang, Time-resolved live-cell spectroscopy reveals EphA2 multimeric assembly, Science 382 (2023) 1042–1050, https://doi.org/10.1126/science.adg5314.

[14] C. Giorgio, I. Hassan Mohamed, L. Flammini, E. Barocelli, M. Incerti, A. Lodola, M. Tognolini, Lithocholic acid is an Eph-ephrin ligand interfering with Eph-kinase activation, PloS One 6 (2011) e18128, https://doi.org/10.1371/journal.pone.0018128.
[15] L. Leng, G. Zhou, A. Liu, H. Wang, Y. Ni, Lithocholic acid species: metabolism, signaling pathways, and clinical significance in enterohepatic diseases, Int. J. Mol. Sci. 26 (2025) 11530, https://doi.org/10.3390/ijms262311530.
[16] M. Tognolini, M. Incerti, I. Hassan-Mohamed, C. Giorgio, S. Russo, R. Bruni, B. Lelli, L. Bracci, R. Noberini, E.B. Pasquale, E. Barocelli, P. Vicini, M. Mor, A. Lodola, Structure–activity relationships and mechanism of action of eph–ephrin antagonists: interaction of cholanic acid with the EphA2 receptor, ChemMedChem 7 (2012) 1071–1083, https://doi.org/10.1002/cmdc.201200102.
[17] D. Pala, R. Castelli, M. Incerti, S. Russo, M. Tognolini, C. Giorgio, I. Hassan-Mohamed, I. Zanotti, F. Vacondio, S. Rivara, M. Mor, A. Lodola, Combining ligand- and structure-based approaches for the discovery of new inhibitors of the EPHA2-ephrin-A1 interaction, J. Chem. Inf. Model. 54 (2014) 2621–2626, https://doi.org/10.1021/ci5004619.
[18] A.G. Temprano, M.R. Romero, A. Ghallab, L. Llera, R.I.R. Macias, H.M. van Eijk, M. Rullán, J. Urman, Ü. Ay, M. Lenicek, J.G. Hengstler, U.P. Neumann, C. Berasain, M.A. Avila, S.W.M. Olde Damink, M.J. Monte, J.J.G. Marin, F.G. Schaap, Gut-to-bile transfer of microbially amidated minor bile acids in patients with hepatopancreatobiliary disorders, Hepatol. Baltim. Md (2025), https://doi.org/10.1097/HEP.0000000000001441.
[19] J.W. Lee, E.S. Cowley, P.G. Wolf, H.L. Doden, T. Murai, K.Y.O. Caicedo, L.K. Ly, F. Sun, H. Takei, H. Nittono, S.L. Daniel, I. Cann, H.R. Gaskins, K. Anantharaman, J.M.P. Alves, J.M. Ridlon, Formation of secondary allo-bile acids by novel enzymes from gut Firmicutes, Gut Microbes 14 (2022) 2132903, https://doi.org/10.1080/19490976.2022.2132903.
[20] Y. Sato, K. Atarashi, D.R. Plichta, Y. Arai, S. Sasajima, S.M. Kearney, W. Suda, K. Takeshita, T. Sasaki, S. Okamoto, A.N. Skelly, Y. Okamura, H. Vlamakis, Y. Li, T. Tanoue, H. Takei, H. Nittono, S. Narushima, J. Irie, H. Itoh, K. Moriya, Y. Sugiura, M. Suematsu, N. Moritoki, S. Shibata, D.R. Littman, M.A. Fischbach, Y. Uwamino, T. Inoue, A. Honda, M. Hattori, T. Murai, R.J. Xavier, N. Hirose, K. Honda, Novel bile acid biosynthetic pathways are enriched in the microbiome of centenarians, Nature 599 (2021) 458–464, https://doi.org/10.1038/s41586-021-03832-5.
[21] W. Li, S. Hang, Y. Fang, S. Bae, Y. Zhang, M. Zhang, G. Wang, M.D. McCurry, M. Bae, D. Paik, E.A. Franzosa, F. Rastinejad, C. Huttenhower, L. Yao, A.S. Devlin, J.R. Huh, A bacterial bile acid metabolite modulates Treg activity through the nuclear hormone receptor NR4A1, Cell Host Microbe 29 (2021) 1366–1377.e9, https://doi.org/10.1016/j.chom.2021.07.013.
[22] Y. Wang, W. Yan, H. Zhao, Y. Lu, Y. Li, S. Peng, Y. Xiao, Isoallolithocholic acid ameliorates intestinal inflammation via metabolically reprogrammed macrophages, Commun. Biol. 8 (2025) 1718, https://doi.org/10.1038/s42003-025-09123-3.
[23] T. Fujii, Y. Nakagawa, K. Funasaka, Y. Hirooka, T. Tochio, Levels of 5α-reductase gene in intestinal lavage fluid decrease with progression of colorectal cancer, J. Med. Microbiol. 73 (2024), https://doi.org/10.1099/jmm.0.001834.
[24] T. Fujii, T. Kuzuya, N. Kondo, K. Funasaka, E. Ohno, Y. Hirooka, T. Tochio, Altered intestinal *Streptococcus anginosus* and 5α-reductase gene levels in patients with hepatocellular carcinoma and elevated bacteroides stercoris in atezolizumab/bevacizumab non-responders, J. Med. Microbiol. 73 (2024), https://doi.org/10.1099/jmm.0.001878.
[25] T.M. Šarenac, M. Mikov, Bile acid synthesis: from nature to the chemical modification and synthesis and their applications as drugs and nutrients, Front. Pharmacol. 9 (2018) 939, https://doi.org/10.3389/fphar.2018.00939.
[26] J.P. Himanen, Y. Goldgur, H. Miao, E. Myshkin, H. Guo, M. Buck, M. Nguyen, K. R. Rajashankar, B. Wang, D.B. Nikolov, Ligand recognition by A-class Eph receptors: crystal structures of the EphA2 ligand-binding domain and the EphA2/ephrin-A1 complex, EMBO Rep. 10 (2009) 722–728, https://doi.org/10.1038/embor.2009.91.
[27] J.P. Himanen, K.R. Rajashankar, M. Lackmann, C.A. Cowan, M. Henkemeyer, D. B. Nikolov, Crystal structure of an Eph receptor-ephrin complex, Nature 414 (2001) 933–938, https://doi.org/10.1038/414933a.
[28] C. Lu, C. Wu, D. Ghoreishi, W. Chen, L. Wang, W. Damm, G.A. Ross, M.K. Dahlgren, E. Russell, C.D. Von Bargen, R. Abel, R.A. Friesner, E.D. Harder, OPLS4: improving force field accuracy on challenging regimes of chemical space, J. Chem. Theory Comput. 17 (2021) 4291–4300, https://doi.org/10.1021/acs.jctc.1c00302.
[29] L. Guidetti, A. Zappia, L. Scalvini, F.R. Ferrari, C. Giorgio, R. Castelli, F. Galvani, F. Vacondio, S. Rivara, M. Mor, C. Urbinati, M. Rusnati, M. Tognolini, A. Lodola, Molecular determinants of EphA2 and EphB2 antagonism enable the design of ligands with improved selectivity, J. Chem. Inf. Model. 63 (2023) 6900–6911, https://doi.org/10.1021/acs.jcim.3c01064.
[30] W.L. Jorgensen, J. Chandrasekhar, J.D. Madura, R.W. Impey, M.L. Klein, Comparison of simple potential functions for simulating liquid water, J. Chem. Phys. 79 (1983) 926–935, https://doi.org/10.1063/1.445869.
[31] T. Darden, D. York, L. Pedersen, Particle mesh Ewald: an N·log(N) method for Ewald sums in large systems, J. Chem. Phys. 98 (1993) 10089–10092, https://doi.org/10.1063/1.464397.
[32] D.R. Roe, T.E. Cheatham, PTRAJ and CPPTRAJ: software for processing and analysis of molecular dynamics trajectory data, J. Chem. Theory Comput. 9 (2013) 3084–3095, https://doi.org/10.1021/ct400341p.
[33] M.P. Jacobson, D.L. Pincus, C.S. Rapp, T.J.F. Day, B. Honig, D.E. Shaw, R. A. Friesner, A hierarchical approach to all-atom protein loop prediction, Proteins 55 (2004) 351–367, https://doi.org/10.1002/prot.10613.
[34] N.-J. Hu, S. Iwata, A.D. Cameron, D. Drew, Crystal structure of a bacterial homologue of the bile acid sodium symporter ASBT, Nature 478 (2011) 408–411, https://doi.org/10.1038/nature10450.
[35] T. Kametani, K. Suzuki, H. Nemoto, First total synthesis of (+)-chenodeoxycholic acid, J. Am. Chem. Soc. 103 (1981) 2890–2891, https://doi.org/10.1021/ja00400a078.
[36] V. Sepe, F.S. Di Leva, C. D'Amore, C. Festa, S. De Marino, B. Renga, M.V. D'Auria, E. Novellino, V. Limongelli, L. D'Souza, M. Majik, A. Zampella, S. Fiorucci, Marine and semi-synthetic hydroxysteroids as new scaffolds for pregnane X receptor modulation, Mar. Drugs 12 (2014) 3091–3115, https://doi.org/10.3390/md12063091.
[37] R. Castelli, M. Tognolini, F. Vacondio, M. Incerti, D. Pala, D. Callegari, S. Bertoni, C. Giorgio, I. Hassan-Mohamed, I. Zanotti, A. Bugatti, M. Rusnati, C. Festuccia, S. Rivara, E. Barocelli, M. Mor, A. Lodola, Δ(5)-Cholenoyl-amino acids as selective and orally available antagonists of the Eph-ephrin system, Eur. J. Med. Chem. 103 (2015) 312–324, https://doi.org/10.1016/j.ejmech.2015.08.048.
[38] S. Russo, D. Callegari, M. Incerti, D. Pala, C. Giorgio, J. Brunetti, L. Bracci, P. Vicini, E. Barocelli, L. Capoferri, S. Rivara, M. Tognolini, M. Mor, A. Lodola, Exploiting free-energy minima to design novel EphA2 protein-protein antagonists: from simulation to experiment and return, Chem. Weinh. Bergstr. Ger. 22 (2016) 8048–8052, https://doi.org/10.1002/chem.201600993.
[39] T. Nishimaki-Mogami, Y. Kawahara, N. Tamehiro, T. Yoshida, K. Inoue, Y. Ohno, T. Nagao, M. Une, 5α-Bile alcohols function as farnesoid X receptor antagonists, Biochem. Biophys. Res. Commun. 339 (2006) 386–391, https://doi.org/10.1016/j.bbrc.2005.11.027.
[40] Y. Iguchi, M. Yamaguchi, H. Sato, K. Kihira, T. Nishimaki-Mogami, M. Une, Bile alcohols function as the ligands of membrane-type bile acid-activated G protein-coupled receptor, J. Lipid Res. 51 (2010) 1432–1441, https://doi.org/10.1194/jlr.M004051.
[41] B. Cerra, F. Venturoni, M. Souma, G. Ceccarelli, A.M. Lozza, D. Passeri, F. De Franco, I.R. Baxendale, R. Pellicciari, A. Macchiarulo, A. Gioiello, Development of 3α,7α-dihydroxy-6α-ethyl-24-nor-5β-cholan-23-sulfate sodium salt (INT-767): process optimization, synthesis and characterization of metabolites, Eur. J. Med. Chem. 242 (2022) 114652, https://doi.org/10.1016/j.ejmech.2022.114652.
[42] C.-W. Hsu, J. Zhao, R. Huang, J.-H. Hsieh, J. Hamm, X. Chang, K. Houck, M. Xia, Quantitative high-throughput profiling of environmental chemicals and drugs that modulate farnesoid X receptor, Sci. Rep. 4 (2014) 6437, https://doi.org/10.1038/srep06437.
[43] A. Macchiarulo, A. Gioiello, C. Thomas, T.W.H. Pols, R. Nuti, C. Ferrari, N. Giacchè, F. De Franco, M. Pruzanski, J. Auwerx, K. Schoonjans, R. Pellicciari, Probing the binding site of bile acids in TGR5, ACS Med. Chem. Lett. 4 (2013) 1158–1162, https://doi.org/10.1021/ml400247k.
[44] J. Wykosky, D.M. Gibo, C. Stanton, W. Debinski, EphA2 as a novel molecular marker and target in glioblastoma multiforme, Mol. Cancer Res. MCR 3 (2005) 541–551, https://doi.org/10.1158/1541-7786.MCR-05-0056.
[45] M.L. Taddei, M. Parri, A. Angelucci, B. Onnis, F. Bianchini, E. Giannoni, G. Raugei, L. Calorini, N. Rucci, A. Teti, M. Bologna, P. Chiarugi, Kinase-dependent and -independent roles of EphA2 in the regulation of prostate cancer invasion and metastasis, Am. J. Pathol. 174 (2009) 1492–1503, https://doi.org/10.2353/ajpath.2009.080473.
[46] Q. Zhao, Z. Duan, R. Lai, P. Ma, Novel microbially transformed bile acids: Biosynthesis, structure, and function, Pharmacol. Res. 216 (2025) 107775, https://doi.org/10.1016/j.phrs.2025.107775.
[47] J. Lin, Q. Nie, J. Cheng, Y.-N. Zhong, T. Zhang, X. Zhang, X. Ge, Y. Ding, C. Niu, Y. Gao, K. Wang, M. Gao, X. Wang, W. Chen, C. Yun, C. Ye, J. Xu, W. Shaoyong, L. Zhang, P. Shang, X. Luo, Z. Zhang, X. Zheng, X. Sha, J. Zhang, S. Nie, X. Zhang, F. Ren, H. Liu, E. Dong, X. Yu, L. Ji, Y. Pang, J.-P. Sun, C. Jiang, A microbial amino-acid-conjugated bile acid, tryptophan-cholic acid, improves glucose homeostasis via the orphan receptor MRGPRE, Cell 188 (2025) 4530–4548.e25, https://doi.org/10.1016/j.cell.2025.05.010.
[48] M. Koolpe, M. Dail, E.B. Pasquale, An ephrin mimetic peptide that selectively targets the EphA2 receptor, J. Biol. Chem. 277 (2002) 46974–46979, https://doi.org/10.1074/jbc.M208495200.
[49] F. Ferlenghi, R. Castelli, L. Scalvini, C. Giorgio, M. Corrado, M. Tognolini, M. Mor, A. Lodola, F. Vacondio, Drug-gut microbiota metabolic interactions: the case of UniPR1331, selective antagonist of the Eph-ephrin system, in mice, J. Pharm. Biomed. Anal. 180 (2020) 113067, https://doi.org/10.1016/j.jpba.2019.113067.
[50] E. Omer, C. Chiodi, Fat digestion and absorption: Normal physiology and pathophysiology of malabsorption, including diagnostic testing, Nutr. Clin. Pract. 39 (2024) S6–S16, https://doi.org/10.1002/ncp.11130.
[51] C. Thomas, A. Gioiello, L. Noriega, A. Strehle, J. Oury, G. Rizzo, A. Macchiarulo, H. Yamamoto, C. Mataki, M. Pruzanski, R. Pellicciari, J. Auwerx, K. Schoonjans, TGR5-mediated bile acid sensing controls glucose homeostasis, Cell Metab. 10 (2009) 167–177, https://doi.org/10.1016/j.cmet.2009.08.001.
[52] E. Martinot, L. Sèdes, M. Baptissart, J.-M. Lobaccaro, F. Caira, C. Beaudoin, D. H. Volle, Bile acids and their receptors, Mol. Aspects Med. 56 (2017) 2–9, https://doi.org/10.1016/j.mam.2017.01.006.
[53] S. Baldi, M. Turrini, F. Cei, M. Menicatti, G. Bartolucci, A. Amedei, Bile acids as key mediators of the gut microbiota-immune axis: potential biomarker and therapeutic perspectives, Biofactors 52 (2026) e70078, https://doi.org/10.1002/biof.70078.
[54] H. Shapiro, A.A. Kolodziejczyk, D. Halstuch, E. Elinav, Bile acids in glucose metabolism in health and disease, J. Exp. Med. 215 (2018) 383–396, https://doi.org/10.1084/jem.20171965.
[55] M. Song, J. Ye, F. Zhang, H. Su, X. Yang, H. He, F. Liu, X. Zhu, L. Wang, P. Gao, G. Shu, Q. Jiang, S. Wang, Chenodeoxycholic acid (CDCA) protects against the lipopolysaccharide-induced impairment of the intestinal epithelial barrier function

via the FXR-MLCK pathway, J. Agric. Food Chem. 67 (2019) 8868–8874, https://doi.org/10.1021/acs.jafc.9b03173.
[56] M. Tognolini, M. Incerti, D. Pala, S. Russo, R. Castelli, I. Hassan-Mohamed, C. Giorgio, A. Lodola, Target hopping as a useful tool for the identification of novel EphA2 protein-protein antagonists, ChemMedChem 9 (2014) 67–72, https://doi.org/10.1002/cmdc.201300305.
[57] F.R. Ferrari, C. Giorgio, A. Zappia, V. Ballabeni, S. Bertoni, E. Barocelli, L. Scalvini, F. Galvani, M. Mor, A. Lodola, M. Tognolini, Pharmacological characterization of second generation FXR agonists as effective EphA2 antagonists: a successful application of target hopping approach, Biochem. Pharmacol. 209 (2023) 115452, https://doi.org/10.1016/j.bcp.2023.115452.
[58] A. Ogawa, T. Murate, M. Suzuki, Y. Nimura, S. Yoshida, Lithocholic acid, a putative tumor promoter, inhibits mammalian DNA polymerase beta, Jpn. J. Cancer Res. Gann 89 (1998) 1154–1159, https://doi.org/10.1111/j.1349-7006.1998.tb00510.x.
[59] M. Genander, J. Frisén, Ephrins and Eph receptors in stem cells and cancer, Curr. Opin. Cell Biol. 22 (2010) 611–616, https://doi.org/10.1016/j.ceb.2010.08.005.
[60] Y. Chen, L. Zhang, Y. Zhang, T. Bai, J. Song, W. Qian, X. Hou, EphrinA1/EphA2 promotes epithelial hyperpermeability involving in lipopolysaccharide-induced intestinal barrier dysfunction, J. Neurogastroenterol. Motil. 26 (2020) 397–409, https://doi.org/10.5056/jnm19095.
[61] H. Zeng, S. Umar, B. Rust, D. Lazarova, M. Bordonaro, Secondary bile acids and short chain fatty acids in the colon: a focus on colonic microbiome, cell proliferation, inflammation, and cancer, Int. J. Mol. Sci. 20 (2019) 1214, https://doi.org/10.3390/ijms20051214.
[62] C. Giorgio, S. Russo, M. Incerti, A. Bugatti, F. Vacondio, E. Barocelli, M. Mor, D. Pala, I. Hassan-Mohamed, A. Gioiello, M. Rusnati, A. Lodola, M. Tognolini, Biochemical characterization of EphA2 antagonists with improved physico-chemical properties by cell-based assays and surface plasmon resonance analysis, Biochem. Pharmacol. 99 (2016) 18–30, https://doi.org/10.1016/j.bcp.2015.10.006.
[63] I. Hassan-Mohamed, C. Giorgio, M. Incerti, S. Russo, D. Pala, E.B. Pasquale, I. Zanotti, P. Vicini, E. Barocelli, S. Rivara, M. Mor, A. Lodola, M. Tognolini, UniPR129 is a competitive small molecule Eph-ephrin antagonist blocking in vitro angiogenesis at low micromolar concentrations, Br. J. Pharmacol. 171 (2014) 5195–5208, https://doi.org/10.1111/bph.12669.
[64] L. Guidetti, R. Castelli, L. Scalvini, F. Ferlenghi, M. Corrado, C. Giorgio, M. Tognolini, A. Lodola, Protein-protein interaction inhibitors targeting the eph-ephrin system with a focus on amino acid conjugates of bile acids, Pharm. Basel Switz. 15 (2022) 137, https://doi.org/10.3390/ph15020137.